IOPscience iopscience.iop.org

Home Search Collections Journals About Contact us My IOPscience

Conductance in double quantum well systems

This article has been downloaded from IOPscience. Please scroll down to see the full text article.

2003 J. Phys.: Condens. Matter 15 R143

(http://iopscience.iop.org/0953-8984/15/4/202)

View the table of contents for this issue, or go to the journal homepage for more

Download details:
IP Address: 171.66.16.119
The article was downloaded on 19/05/2010 at 06:30

Please note that terms and conditions apply.

INSTITUTE OF PHYSICS PUBLISHING JOURNAL OF PHYSICS: CONDENSED MATTER

J. Phys.: Condens. Matter **14** (2002) R143–R175 PII: S0953-8984(02)28907-9

TOPICAL REVIEW

Conductance in double quantum well systems

J E Hasbun

Department of Physics, State University of West Georgia, Carrollton, GA 30118, USA

E-mail: jhasbun@westga.edu

Received 2 August 2002
Published 20 January 2003
Online at stacks.iop.org/JPhysCM/14/R143

Abstract
The object of this paper is to review the electronic conductance in double quantum well systems. These are quantum well structures in which electrons are confined in the z direction by large band gap material barrier layers, yet form a free two-dimensional Fermi gas within the sandwiched low band gap material layers in the x–y plane. Aspects related to the conductance in addition to the research progress made since the inception of such systems are included. While the review focuses on the tunnelling conductance properties of double quantum well devices, the longitudinal conductance is also discussed. Double quantum well systems are a more recent generation of structures whose precursors are the well known double-barrier resonant tunnelling systems. Thus, they have electronic signatures such as negative differential resistance, in addition to resonant tunnelling, whose behaviours depend on the wavefunction coupling between the quantum wells. As such, the barrier which separates the quantum wells can be tailored in order to provide better control of the device's electronic properties over their single well ancestors.

Contents

1. Introduction 144
2. Theoretical approaches to transport 148
   2.1. Longitudinal conductance 149
   2.2. Tunnelling conductance—the Wigner and Landauer approaches 151
3. Numerical applications 153
   3.1. Non-self-consistent and self-consistent method 153
   3.2. Application to double-barrier (single well) system 157
   3.3. Application to the triple-barrier (double well) system 162
4. Inclusion of the magnetic field 163
   4.1. Magnetic field in the direction of the tunnelling current 163
   4.2. Magnetic field in the plane of the layers 166

0953-8984/02/040143+33$30.00 © 2002 IOP Publishing Ltd Printed in the UK

5. Conclusion 172
Acknowledgments 173
References 173

1. Introduction

The technological significance of efficient, small size and fast response electronic components is responsible for much of the research in quantum well structures. The ability to grow high quality crystalline semiconductor structures over the past decades has been made possible by the molecular beam epitaxy (MBE) technique [1]. This technique ushered in the age of layered semiconductor structures that are nearly perfect on an atomic scale and hence have dimensions comparable to that of a traversing electron's mean free path and the de Broglie wavelength.

Heterostructures [1, 2], quantum wells [3, 4] and superlattices [4, 5] are examples of low-dimensional systems where size plays a fundamental role as regards the electronic properties of two-dimensional electron gas (TEG) [6] devices. The realization of these, as well as one-dimensional quantum wire [7] and zero-dimensional quantum dot [8] structures, were proposed more than two decades ago [9].

The double quantum wells, which is the subject of this review, fall in the TEG category. The essential advantage of a TEG system is that impurities can be removed from the plane of the mobile electrons. The charge carriers can thus achieve high mobilities in, for example, modulation doped structures consisting of GaAs/AlGaAs materials [10]. Mobilities greater than 10^6 cm^2 V^{-1} s^{-1} reported in the early 1980s had been surpassed with values exceeding 10^7 cm^2 V^{-1} s^{-1} by the late 1980s and early 1990s [9–13]. These structures consist of ultrathin layers of GaAs and AlGaAs grown on one another periodically. The materials' different band gaps present discontinuities in real space. Electrons and holes in these quantum well structures show one-dimensional behaviour normal to the layers and the quantization of the carriers' motions in this direction produces a set of discrete energy levels. This is not unlike that presented in introductory quantum mechanical one-dimensional wells and barriers [14]. In the direction parallel to the layers the electrons manifest a two-dimensional behaviour. The reduced dimensionality induces drastic changes in the electrical and optical properties of quantum well structures. For example, referring to figure 1, where a quantum well structure diagram of GaAs/AlGaAs is depicted, the introduction of impurities in the high band gap AlGaAs layers, in such a way that the impurity nuclei are trapped while the carriers that are introduced can migrate toward the low gap GaAs layers, is thus responsible for producing a TEG at the interface. The high mobilities that are achieved in the modulation doped samples [9] are due to the high density of electrons in the GaAs conduction channels (x–y plane) and the reduced impurity scattering. The successful growth of high quality quantum well structures was demonstrated in the early 1980s using different materials such as in GaAs/AlGaAs by MBE [15], InGaAs/AlInAs by vapour phase epitaxy (VPE) [16] and organo-metallic chemical vapour deposition (OMCVD) [17].

During the early 1970s, Esaki and Tsu [4, 18], in anticipation of advances in epitaxy, proposed research on an engineered semiconductor superlattice. Here the authors envisioned nanostructures with alternating layers of high and low gap materials, i.e. a series of quantum wells (figure 1) adjacent to each other as a superlattice. Their analysis of the electron dynamics in the z direction predicted unusual current–voltage characteristics, including negative differential conductance and negative differential resistance (NDR) [18]. This refers to a drop in current with an increase in voltage, i.e. if we write $I = GV$ then the conductance, G, corresponds to a negative slope in the I–V sample characteristics. Esaki *et al* [4, 19] found that an MBE grown GaAs/GaAlAs superlattice indeed exhibited a negative resistance ($1/G$)

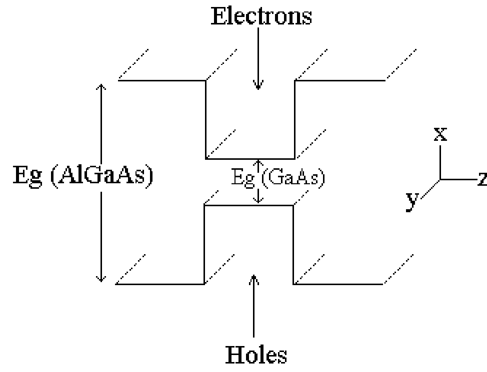

Figure 1. A quantum well structure with two layers of the low gap GaAs material sandwiched between two layers of the higher gap AlGaAs material. The quantized motion is along the z direction.

in its transport properties. Led by the computation of the resonant transmission coefficient as a function of electron energy for multibarrier structures from a tunnelling point of view [20], Chang *et al* [21] observed resonant tunnelling in a MBE grown double-barrier quantum system. The current and conductance versus voltage curves for their system is shown in figure 2. The figure shows an inset with a double-barrier potential well system with two resonances at energies E_1 and E_2. The meaning of resonant levels is that, if the thickness of the barriers (80 Å) were made infinitely large, then those states would represent true states of an electron in an attractive square well [22]. In figure 2 the resonant tunnelling occurs at the current maxima for which the applied voltages are such that the Fermi energy of the electrode coincides with the resonant states. The applied voltage bends the potential well systems and the energy positions depend on the voltage according to solutions of the Schrödinger equation. In their work [21] the resonant voltage positions are found at approximately twice the state energies. At such voltage values the electrons tunnel unimpeded across the potential barrier, from one electrode to the other. This is reasonable because if, for example, we assume a one-level quantum well system with a resonant energy as a function of voltage written as $E_0' = -\frac{\hbar^2}{2m}\langle\psi'|\frac{\partial^2}{\partial x^2}|\psi'\rangle + \langle\psi'|V_b + V(z)|\psi'\rangle \simeq E_0 + \langle\psi|V(z)|\psi\rangle$, where ψ' is the wavefunction of the system in the presence of the voltage $V(z)$ and ψ is the wavefunction of the system in its absence, under the influence of the barrier potential V_b alone, with eigenstate E_0, then for small voltage with $\psi' \sim \psi$, the energy shift is given by the average of the potential across the well width d. Writing, $V(z) = -\frac{eV}{d}z$, we see that the energy shift $E_0' - E_0 \sim -\frac{eV}{2}$, since $\langle z\rangle = \frac{d}{2}$, so that when E_0' approaches the Fermi level, E_F, of the incident electron's side ($E_0' = E_F \equiv 0$) a resonance would occur at approximately $eV = 2E_0$. While Chang *et al* [21] observed resonant tunnelling at low temperature, Sollner *et al*'s work clearly showed large regions of NDR [23] mentioned earlier [18]. The significance of a NDR region in the I–V characteristics of a device, as shown in figure 3, suggests that such devices are useful as amplifiers and oscillators [23–26]. In fact, by the late 1980s oscillator frequencies in the hundreds of gigahertz range were reported [26]. From a simple classical point of view, one way to see how it is possible for a NDR device, with I–V characteristics similar to figure 3, to give rise to charge oscillations is to write the device's current versus voltage as

$$I = G(V)V, \tag{1}$$

where the conductance, G, is a function of the voltage, to find

$$\frac{\mathrm{d}I}{\mathrm{d}t} = v_d \left(V \frac{\mathrm{d}G}{\mathrm{d}V} + G \right) \frac{\mathrm{d}V}{\mathrm{d}z}, \tag{2}$$

where v_d is the electronic drift velocity. Using Poisson's equation, $E(z) = -\frac{\mathrm{d}V}{\mathrm{d}z} = \frac{q}{\epsilon} N_s(z)$, with N_s the areal electron density at position z, we see that the electronic charge obeys the equation

$$\frac{\mathrm{d}^2 q}{\mathrm{d}t^2} + \omega(z)^2 q = 0, \tag{3}$$

where $\omega(z) \equiv \sqrt{v_d (V \frac{\mathrm{d}G}{\mathrm{d}V} + G) \frac{N_s(z)}{\epsilon}}$, in the present understanding, is a frequency dispersion relation which becomes imaginary for negative differential conductance ($1/R$) whenever $\frac{\mathrm{d}G}{\mathrm{d}V} < -\frac{G}{V}$. The charge builds up within the sample at such a characteristic rate when it is operated in the NDR region. The charge spike travels along the sample and then decays. The actual number of spikes that reach from one side of the sample to the other is the charge frequency associated with oscillators of this type; that is v_d/ℓ, where ℓ is the sample length of travel. Such oscillations in semiconductor devices have been of interest for many years [27] in connection with Gunn diodes [28]. According to Brown *et al* [26], the maximum frequency of operation of the resonant tunnelling type structures depends on the device's I–V peak to valley ratio (see figure 3). The higher the ratio the higher the operating frequency. Further significant applications of resonant tunnelling structures include logic circuits and memory cells [29] and single-electron transistors [30, 31].

A natural extension of a double-barrier tunnelling system is the two coupled wells or triple-barrier system shown in figure 4. Here two individual wells are coupled through a barrier. Depending on the thickness of the middle barrier the system's eigenstates depend on the wavefunction overlap between the two wells. In fact, the first observation of the energy splitting obtained in a triple-barrier system, with a thin middle barrier, was reported over a decade ago [32] using resonant tunnelling spectroscopy [5, 23]. The interest in this more recent class of quantum wells is due to the ability to tailor the middle barrier and permit the investigation of quantum phenomena [32], including electron–electron interactions [33] and the Coulomb gap [34]. Furthermore, in order to improve the ability to control the tunnelling process and thereby create transistor action, the third layer, i.e. the middle barrier, is added to the standard double-barrier system, thus creating two separate wells [35]. These two quantum wells host electrons whose behaviour is two-dimensional. Modulating the tunnelling between the two wells allows the system's conductance properties to be investigated [35, 36] in the so-called double electron layer transistors [36]. Such devices still develop NDR due to their resonant tunnelling features, have high peak to valley I–V properties and have been demonstrated to show bistable memory [37], yet are an improvement over their double-barrier ancestors due mainly to their middle barrier control layer. It has been recently reported that size-induced strain in triple-barrier structures can be used to provide additional control over the quantum coupling between the double wells, which in turn affects their conductance properties [38].

It should be noted that, while double quantum well systems come in triple [32] or single [35] barriers, for example, in this review no rigorous distinction will be addressed between them due to their similarity. As far as this review is concerned the difference in their electronic behaviour is an open question. In section 2 we discuss theoretical approaches to the study of transport applicable to resonant tunnelling systems. In section 3, typical calculations on a double-barrier system are carried out which are later extended to the double well system of interest here. The double-barrier calculations are performed in the presence of an applied

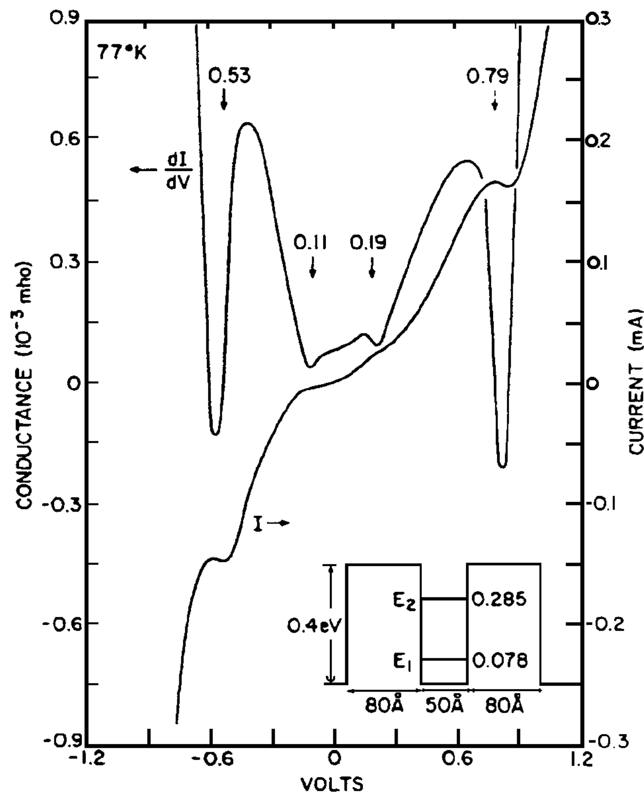

Figure 2. Current and conductance characteristics of a double barrier structure of GaAs between two $Ga_{0.3}Al_{0.7}As$, as shown in the energy diagram. Both the thicknesses and the calculated quasi-stationary states of the structure are indicated in the diagram. Arrows in the curves indicate the observed voltages of singularities corresponding to these resonant states [21]. Copyright (1974) by the American Institute of Physics. Reprinted with permission of AIP and the authors.

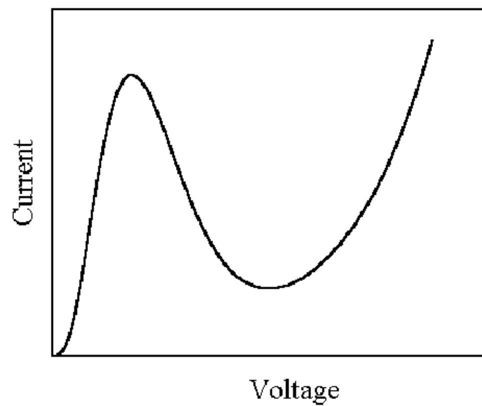

Figure 3. An example of a typical current–voltage characteristic behaviour of a quantum well device that exhibits negative differential resistance. The current peak position is related to the quantized level structure of the device.

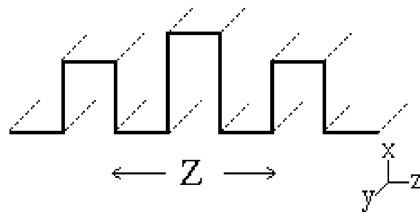

Figure 4. Double well or triple-barrier system. The quantized motion is due to the confinement along the z direction. Tunnelling occurs between the two wells through the middle barrier.

voltage and a comparison is made between theory and experiment. In section 4 extensions to include the effect of the magnetic field are discussed and we conclude in section 5.

2. Theoretical approaches to transport

Since the discovery in the early 1960s of active semiconductor devices capable of converting direct current to coherent microwave oscillations, one of the major efforts in semiconductor technology has been the development of electronic devices operating at high power densities and high frequencies while simultaneously being reduced in size. Gate lengths in the submicron range [39] and even smaller can be achieved [9]. Because of the high electric fields and ultra-small dimensions encountered in present semiconductor devices, the time scales involved mean that major modifications are required to the traditional Boltzmann transport theoretical approach [40–42].

The classical Boltzmann transport equation (BTE) has played a very significant role in the early development of solid state physics. In the last decades as the semiconductor technology downscales the integrated circuits into submicron regions, there has been a strong need to develop fundamental approaches to quantum transport [40, 42]. In the BTE, the collision terms are derived under the assumption that electron scattering occurs instantaneously. This is a reasonable approximation when the mean time between collisions is large. However, in small devices the duration of the collision process is finite, so that the use of the BTE is questionable [42, 43]. Examples of challenging transport phenomena are the hot electron effect [44, 45], transient transport [46], ballistic transport [47], velocity overshoot [48], quantum size effect [49] and a host of various problems associated with hot carriers in semiconductors [50]. In addition to Monte Carlo methods [51] and energy–momentum equation schemes [46, 52] transport properties have been investigated theoretically by several approaches [40, 42, 53]. Reviews on various schemes to investigate transport in miniature scale systems have appeared in the literature over the years. Methods that make use of the Kubo formula [54], the path integral [55], the Green function [56], the Wigner function [57] and the Landauer formula (LF) [53, 58] have been discussed in the literature [53], including the Monte Carlo approach [59]. For the purposes of this review we will concentrate on the methods that, for the most part, have been applied to resonant tunnelling double-barrier systems and could easily be extended to tunnelling conductance studies in double well systems. One of these is the Wigner function approach [57] which was applied to double-barrier systems early on [60], reviewed in the early 1990s [53, 61], and more recently applied to simulations of quantum transport in resonant tunnelling systems [62–64]. Also of great use is the Landauer formulation mentioned earlier [58] and which has gained popularity in recent years [65–68]. It is important to mention that, while much less popular, the path integral approach [55] has, in fact, found applications [69] in our systems of interest, and similarly has a Monte Carlo scheme [70]; these approaches, however, are not discussed in this review any further.

2.1. Longitudinal conductance

This review is mainly focused on tunnelling conductance; however, it is important to discuss significant conductance properties in double well systems in the longitudinal direction, i.e. the direction along the quantum well layers (x–y plane). Under an applied voltage, electrons in a semiconductor sample respond to produce a current proportional to the applied voltage. The current is written as

$$I = GV, \tag{4}$$

where the conductance is defined as

$$G = \frac{\mathrm{d}I}{\mathrm{d}V} \tag{5a}$$

and the average conductance as

$$\overline{G} = \Delta I/\Delta V. \tag{5b}$$

The conductance is equivalent to the inverse of the resistance or it can be related to the conductivity of a sample by the relation $G = \sigma A/\ell$ with A and ℓ the sample area and length of interest. The difference being a geometric factor. Its relationship to the mobility μ is

$$G = \frac{A}{\ell} ne\mu, \tag{6}$$

where n is the density of electrons and e is the electronic charge. The mobility is related to the scattering lifetime, τ, as $\mu = \frac{e}{m}\langle\tau\rangle$, where $\langle\tau\rangle$ is the averaged scattering lifetime defined [71, 72] as

$$\langle\tau\rangle = \frac{\sum_k \varepsilon_k \tau_k F'(\varepsilon_k)}{\sum_k \varepsilon_k F'(\varepsilon_k)}, \tag{7}$$

where $F'(\varepsilon_k)$ is the derivative of the Fermi distribution function with respect to the band energy ε_k and τ_k is related to the scattering rate defined [71–73] as

$$\frac{1}{\tau_k} = \sum_{k'} W_{kk'}(1 - \cos\theta_{kk'}), \tag{8}$$

with the scattering rate from state k to k' given by

$$W_{kk'} = \frac{2\pi}{\hbar}|H_{kk'}|^2 \delta(\varepsilon(k') - \varepsilon(k)) \tag{9}$$

and $H_{kk'}$ is the matrix element due to the scattering potential responsible for limiting the motion. This can be due to impurities, phonons, surface roughness, etc [72, 74–76]. The longitudinal current density under an electric field E is $J = nev$ where $v = \mu E$. We note that in equation (9) the matrix element can be carried out with the full knowledge of the problem's wavefunction; that is, by a full solution of the Schrödinger equation. This will be discussed below in section 3. Furthermore, there are two kinds of motions associated with a double quantum well problem. One is the motion along the quantum well channels due to the presence of a longitudinal field, say along the x or y direction in figure 4. The longitudinal motion can actually be quite complicated. The reason is that the channels can contribute to the motion in different ways. For example, the discovery of resistance resonance in the early 1990s [77] has given rise to a flurry of activity [78–81] in this area. The significance of that work [77] can be summarized by the expression [82] for the conductivity:

$$\sigma = \sigma_0(1 + F_\mu), \qquad \sigma_0 = \frac{e^2 n}{m}\tau, \qquad F_\mu = \frac{\mu^2(1+\delta^2)}{(1-\mu^2)(1+\delta^2)+t^2}, \tag{10}$$

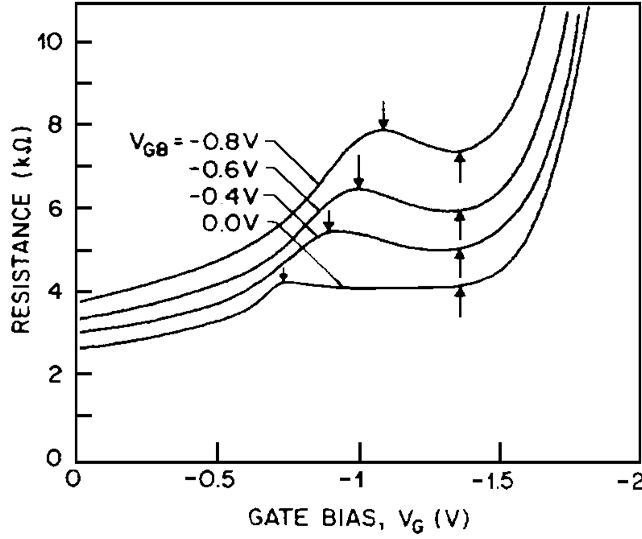

Figure 5. Resistance versus gate bias characteristics (back-gated structure) at 4.2 K at different values of the back-gate bias (V_{GB}). The bias across the channel was 4 mV. The downward arrows indicate the position of the resistance resonance: the upward ones show the starting point of the second well depletion [77]. Copyright (1990) by the American Physical Society. Reprinted with permission of APS and the authors.

with $1/\tau = \frac{1}{2}\left[\frac{1}{\tau_r} + \frac{1}{\tau_l}\right]$ and τ_r, τ_l are associated with each well's scattering lifetime as discussed above. Also, δ is a measure of the resonant state splitting energy of each well, t is a measure of their coupling and $\mu \equiv (\tau_r - \tau_l)/(\tau_r + \tau_l)$. Thus, when the coupling between the two wells is very small, due to a wide or tall middle barrier, each well acts independently of the other. In which case $t \to 0$, $F_\mu \to \frac{\mu^2}{(1-\mu)(1+\mu)}$ and the conductivity is obtained as

$$\sigma = \frac{e^2 n}{2m}(\tau_r + \tau_l). \tag{11}$$

This indicates that the two wells act as if they were conductors in parallel with additive scattering lifetimes. However, if the middle barrier is narrow or small and the two wells are more strongly coupled, then t is large so that F_μ is small and we obtain

$$\sigma \sim \sigma_0 = \frac{\tau_l \tau_r}{\tau_l + \tau_r}. \tag{12}$$

In such a case the two wells act as if they were conductors in series with the scattering rates now being additive as in Mathiessen's rule [83]. Palevski *et al* [77] demonstrated the resistance resonance by varying the applied voltage along the z direction in order to change the energy splitting between the states in the wells. Their results are shown in figure 5. While the above equations (7)–(9) were written in the Born approximation [72] and equations (10)–(12) were obtained through the use of the Kubo formula [53, 54], as mentioned before other approaches are possible [51–61]. Additionally, more specific methods applicable to study transport properties in double wells have begun to appear in the literature [84, 85].

Other examples of problems dealing with the longitudinal motion of electrons in double well systems include electron–electron interaction [33, 34, 86] studies, the frictional drag between the middle barrier separated electrons in the absence of a magnetic field [87] and in strong magnetic fields [88].

2.2. Tunnelling conductance—the Wigner and Landauer approaches

The majority of the excitement associated with double quantum wells deals with the resonant tunnelling characteristics as mentioned in the introduction. The electronic motion is now along the z direction of figure 4. The interest now is in the tunnelling current. As mentioned above, the Wigner distribution function [53, 57, 61–64] has been employed in the study of resonant tunnelling systems. Here the starting point is the variable effective mass Hamiltonian [60, 61, 63, 89] given by

$$H(z) = -\frac{\hbar^2}{2m}\frac{\mathrm{d}}{\mathrm{d}z}\left(\frac{1}{m(z)}\frac{\mathrm{d}}{\mathrm{d}z}\right) + v(z), \tag{13}$$

where $v(z)$ is the double well potential, as will be discussed later below. The idea in the Wigner method [89] is to write the Liouville equation for the density matrix as

$$\frac{\partial \rho(z, z')}{\partial t} = \frac{\mathrm{i}}{\hbar}(H(z) - H(z'))\rho(z, z'), \tag{14}$$

with the density matrix given by

$$\rho(z, z') = \sum_i P_i \Phi_i(z)\Phi_i^*(z'), \tag{15}$$

where P_i is the ith state occupation probability and $\Phi_i(z)$ is the ith state wavefunction. The change of variables

$$Z = \tfrac{1}{2}(z + z'), \qquad \xi = z - z', \tag{16}$$

is usually made in order to define the Wigner function as the Fourier transform of the density matrix:

$$f(Z, k) = \int_{-\infty}^{\infty} \mathrm{d}\xi\, \mathrm{e}^{\mathrm{i}k\xi} \rho(Z + \tfrac{1}{2}\xi, Z - \tfrac{1}{2}\xi). \tag{17}$$

The partial differential equation that results for the Wigner function is given [60] by

$$\frac{\partial f}{\partial t} = -\frac{\hbar k}{m}\frac{\partial f}{\partial z} - \frac{1}{\hbar}\int_{-\infty}^{\infty}\frac{\mathrm{d}k'}{2\pi} V(Z, k - k') f(Z, k'), \tag{18}$$

where

$$V(X, k) = 2\int_0^{\infty} \mathrm{d}\xi\, \sin(k\xi)[v(Z + \tfrac{1}{2}\xi) - v(Z - \tfrac{1}{2}\xi)]. \tag{19}$$

In addition to normalizing the Wigner function and the density matrix, $n(Z) = \rho(Z, Z) = \int_{-\infty}^{\infty} \frac{\mathrm{d}k}{2\pi} f(Z, k)$, so as to represent the electron density $n(Z)$, so that $f(Z, k)$ is solved self-consistently, coupled to the Poisson equation

$$\frac{\partial}{\partial Z}\left(\epsilon \frac{\partial \phi}{\partial Z}\right) = -e[\Gamma(Z) - n(Z)], \tag{20}$$

where Γ is the impurity density and the potential $\phi(Z)$ is related to $v(Z)$ through $v(Z) = -[\Upsilon_e(Z) - \Upsilon_e(0)] - e[\phi(Z) - \phi(o)]$, where Υ_e is the electron affinity in the semiconductor and with suitable boundary conditions [60]. Finally, the current density can be obtained from the Wigner function as

$$J(Z) = e\int_{-\infty}^{\infty} \frac{\mathrm{d}k}{2\pi} \frac{\hbar k}{m(Z)} f(Z, k). \tag{21}$$

The popularity of the Wigner function approach stems from its resemblance to the Boltzmann distribution function approach [71], with the basic difference that the Heisenberg uncertainty principle is obeyed. Results obtained for the current density using the Wigner

function in a resonant tunnelling system by Kim and Lee [63] will be shown in section 3. The Landauer approach [58], in contrast to the Wigner function, is conceptually simpler. While the LF has been rigorously obtained through the Kubo formula [65, 90], it is possible to obtain it through the standard definition of average current [91]:

$$\vec{I} = e\,T_r(n\vec{v}) = \frac{eA}{(2\pi)^3}\sum_{\sigma}\int \mathrm{d}^3k\, F_\sigma(\vec{k})\vec{v}_\sigma(\vec{k}) = \frac{2eA}{(2\pi)^3}\int \mathrm{d}^3k\, F(\vec{k})\vec{v}(\vec{k}), \tag{22}$$

where T_r is the trace and the spin sum has been carried out, $\vec{v}(\vec{k})$ is the velocity and $F(\vec{k})$ is the Fermi distribution function. For the structures of interest in this review (figures 1 and 4), let F_A represent the equilibrium distribution on the left side of the structure where electrons are incident from, and let F_B represent that of the right side. The velocity is related to the band energy as

$$\vec{v}(\vec{k}) = \frac{1}{\hbar}\vec{\nabla}_k\varepsilon(k). \tag{23}$$

Further, writing the total amplitude or probability of electron transmission from the A side to the B side as $F_A(1 - F_B)T(\vec{k})$; that is, a product of the probability that a state on the A side is occupied times the probability that a state on the B side is empty times the tunnelling probability $T(\vec{k})$. Finally, replacing $F(\vec{k})$ in equation (22) with the above total amplitude and using equation (23), we get the total current from the A to the B side as

$$\vec{I}_{AB} = \frac{2eA}{(2\pi)^3\hbar}\int \mathrm{d}^3k\, T_{AB}F_A(1 - F_B)\vec{\nabla}_k\varepsilon(k), \tag{24}$$

with a similar expression for I_{BA} for the current from side B to side A. Since by symmetry $T_{AB} = T_{BA} \to T$, the net current is

$$\vec{I} = \vec{I}_{AB} - \vec{I}_{BA} = \frac{2eA}{(2\pi)^3\hbar}\int \mathrm{d}^3k\, T(\vec{k})[F_A(\vec{k}) - F_B(\vec{k})]\vec{\nabla}_k\varepsilon(k). \tag{25}$$

If we write $\vec{k} = k_\parallel\hat{\parallel} + k_\perp\hat{\perp}$; that is, with parallel and perpendicular components as in a cylindrical energy surface [91], then $\mathrm{d}^3k = \mathrm{d}S_\varepsilon\,\mathrm{d}\varepsilon/|\vec{\nabla}_k\varepsilon(k)|$, where $\mathrm{d}s_\varepsilon(= \mathrm{d}^2k_\parallel)$ is a cylindrical cap area of k space with the cylinder's length $\mathrm{d}k_\perp = \mathrm{d}\varepsilon/|\vec{\nabla}_k\varepsilon(k)|$, we obtain the current as

$$\vec{I} = \frac{2eA}{(2\pi)^3\hbar}\int \mathrm{d}S_\varepsilon\int \mathrm{d}\varepsilon\, T(k_\parallel,\varepsilon)[F_A(k_\parallel,\varepsilon) - F_B(k_\parallel,\varepsilon)]\hat{n}_{v(k_\parallel,k_\perp)}, \tag{26}$$

where $\hat{n}_{v(k_\parallel,k_\perp)} = \vec{\nabla}_k\varepsilon(k)/|\vec{\nabla}_k\varepsilon(k)|$ has been used. Furthermore, we write $F_i(k_\parallel,\varepsilon) = (1 + \exp[(\varepsilon_{k_\parallel} + \varepsilon - E_{Fi} + e\phi_i)/KT])^{-1}$, where $\varepsilon_{k_\parallel} = (\hbar k_\parallel)^2/2m$, $\varepsilon = (\hbar k_\perp)^2/2m$ and ϕ_i is the bias voltage applied on the side i which takes on the values A or B for the left and right sides, respectively. In addition to neglecting the plane motion dependence of the transmission coefficient, so that $T(k_\parallel,\varepsilon) \to T(\varepsilon)$ and similarly for the F_i's, the two-dimensional integral can be performed, $\int \mathrm{d}S_\varepsilon = (2\pi)^2/A$, to obtain the LF [65–68] for the current in the z direction ($\hat{n}_v \to \hat{z}$) as

$$I_{LF} = \frac{2eA}{2\pi\hbar}\int T(\varepsilon)[F_A(\varepsilon) - F_B(\varepsilon)]\,\mathrm{d}\varepsilon. \tag{27}$$

It is worth noting that, if in equation (26) we make the replacement for $T(k_\parallel,\varepsilon) \to T(\varepsilon)$ as done above, but keep $F(k_\parallel,\varepsilon)$ as shown, then it is possible to perform the integral using $\int_0^\infty \mathrm{d}s_\varepsilon = \int_0^{2\pi}\int_0^\infty k_\parallel\,\mathrm{d}k_\parallel\,\mathrm{d}\theta = \frac{2\pi m}{\hbar^2}\int_0^\infty \mathrm{d}\varepsilon_\parallel$:

$$\int_0^\infty \mathrm{d}S_\varepsilon[F_A(k_\parallel,\varepsilon) - F_B(k_\parallel,\varepsilon)] = \frac{2\pi m}{\beta\hbar^2}\ln\left\{\frac{1+\exp[-\beta(\varepsilon + e\phi_A - E_{FA})]}{1+\exp[-\beta(\varepsilon + e\phi_B - E_{FB})]}\right\} = \frac{2\pi m}{\beta\hbar^2}F(\varepsilon), \tag{28}$$

where $F(\varepsilon)$ is referred to as the supply function [5, 76] and $\beta = 1/KT$, to obtain the standard tunnelling theory (STT) total current in the z direction [5]:

$$I_{STT} = \frac{emAKT}{2\pi^2\hbar^3} \int d\varepsilon\, T(\varepsilon) F(\varepsilon). \tag{29}$$

Comparing equations (27) and (29) it is seen that the LF appears to ignore the dependence on $\varepsilon_\parallel$ in the Fermi distribution functions, which seems reasonable in the absence of coupling between plane and transverse motion. This may perhaps be a more drastic approximation in the presence of a magnetic field [92, 93]. We will come back to this subject later. Equation (27) is generally referred to as the non-linear form of the LF [66]. There is a linear form that helps to understand resonant tunnelling in a one-level system. For example, at low voltage differences between the B and A sides of the device, we can replace the Fermi function difference in equation (27) with

$$F_A(\varepsilon) - F_B(\varepsilon) \simeq F'_B(\varepsilon)\Delta V, \tag{30}$$

where $\Delta V = E_{FA} - E_{FB} - e\Delta\phi$, with $\Delta\phi = \phi_A - \phi_B$. At low temperatures $-F'_B(\varepsilon)$ is a delta function, and taking $\phi_B \sim -\Delta\phi$ as well as $E_{FB} \to E_F$, $E_{FA} \equiv 0$, $\phi_A \equiv 0$, so that $\Delta V \to -E_{FB} - e\Delta\phi$ to obtain from equation (27) in this limit

$$I \approx -\frac{e\Delta V}{\pi\hbar} \int T(\varepsilon)\delta(\varepsilon - e\Delta\phi - E_F)\, d\varepsilon = \frac{e\Delta V}{\pi\hbar} T(E_F + e\Delta\phi). \tag{31}$$

That is, if $E_F + e\Delta\phi = E_r$, with E_r being a resonant level at bias $\Delta\phi$ in the quantum well between the barriers, there will be a large contribution to the current. This is the same resonant condition idea discussed earlier in the introduction. The resonant level, E_r, depends on the applied voltage however. This resonance condition is shown in figure 6. Nevertheless, under general conditions, $T(\varepsilon)$ is a function of the electric field and also the Fermi function difference has wider implications. At any particular value of the electric field, the Fermi function broadens as the temperature is increased and we expect the conductance will similarly decrease with temperature as $F_A(\varepsilon) - F_B(\varepsilon) \simeq 1/T$. For large electric field, E, we can write $F_A(E) - F_B(E) \simeq F_A(E)$, due to the vanishing of $F_B(E)$ at large field or voltage $\phi = E\ell$, with ℓ the sample biasing length, so that the average conductance from equations (5) and (27), in this limit, behaves as $G \sim 1/E$.

Comparison between the LF, the Wigner function and the STT is carried out in the next section where a numerical approach developed recently [94] will be employed.

3. Numerical applications

In this section a numerical approach to obtain the conductance [94] in quantum well systems will be used. The approach has been tested and compared with an earlier transfer matrix method [95] in good agreement. Below, results based on calculations using the LF and the STT of equations (27) and (29) are shown. The results will ultimately be compared with Wigner function results in a double-barrier resonant tunnelling system. Similar calculations will be given for the double well system, where Wigner function results have not yet been reported in the literature.

3.1. Non-self-consistent and self-consistent method

The Schrödinger equation for the general potential of figure 7 is broken into three parts, one for each region shown in the figure. Regions I and II have plane wave solutions, and there

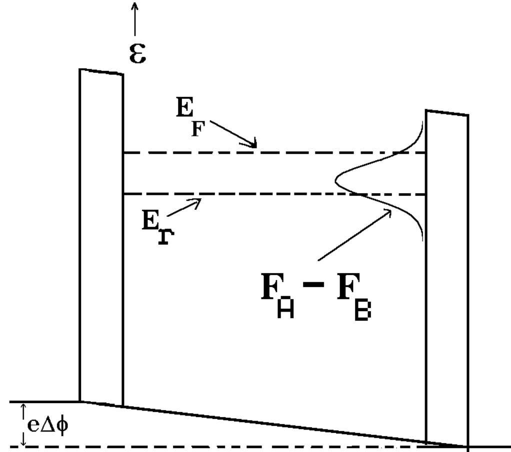

Figure 6. The Fermi function difference, F_A–F_B, at low field and low temperature is shown to overlap with a level in the well. The resonant condition is such that $E_r = E_F + e\Delta\phi$, where $\Delta\phi = \phi_A - \phi_B$.

remains region II where the potential, $V_2(z)$, is assumed to be of any shape. In that region, we write

$$-\frac{\hbar^2}{2m}\frac{\partial^2}{\partial z^2}\psi(\varepsilon, z) + V_2(z)\psi(\varepsilon, z) = \varepsilon\psi(\varepsilon, z). \tag{32}$$

Later, region II will be specialized to a specific shape, i.e. double barrier or triple barrier. We next assume a solution of the form

$$\psi = \begin{cases} \psi_I = A_1 \exp(\mathrm{i}k_1 z) + B_1 \exp(-\mathrm{i}k_1 z) & \text{for } z < \alpha \\ \psi_{II} = A_2\, f(z) + B_2 g(z) & \text{for } \alpha < z < \beta \\ \psi_{III} = A_3 \exp(\mathrm{i}k_3 z) + B_3 \exp(-\mathrm{i}k_3 z) & \text{for } z > \beta, \end{cases} \tag{33}$$

for regions I, II and III of figure 7, respectively, and the functions $f(z)$ and $g(z)$ are to be obtained as explained below. With the standard use of boundary conditions for the wavefunction, the following relations are obtained [94]:

$$\begin{pmatrix} A_1 \\ B_1 \end{pmatrix} = \begin{pmatrix} t_{11} & t_{12} \\ t_{21} & t_{22} \end{pmatrix} \begin{pmatrix} A_3 \\ B_3 \end{pmatrix}, \tag{34}$$

and since there is no reflection from region III, $B_3 \equiv 0$. The final results for the reflection and transmission coefficients are given as

$$R = \frac{|t_{21}|^2}{|t_{11}|^2}, \qquad T = 1 - R, \tag{35a}$$

where

$$t_{11} = \frac{\mathrm{e}^{\mathrm{i}(k_3\beta - k_1\alpha)}}{2}\left\{\left[f(\alpha) + \frac{f'(\alpha)}{\mathrm{i}k_1}\right]\left[\frac{g'(\beta) - \mathrm{i}k_3 g(\beta)}{f(\beta)g'(\beta) - g(\beta)f'(\beta)}\right] + \left[g(\alpha) + \frac{g'(\alpha)}{\mathrm{i}k_1}\right]\left[\frac{f'(\beta) - \mathrm{i}k_3 f(\beta)}{f'(\beta)g(\beta) - g'(\beta)f(\beta)}\right]\right\}, \tag{35b}$$

$$t_{21} = \frac{\mathrm{e}^{\mathrm{i}(k_3\beta + k_1\alpha)}}{2}\left\{\left[f(\alpha) - \frac{f'(\alpha)}{\mathrm{i}k_1}\right]\left[\frac{g'(\beta) - \mathrm{i}k_3 g(\beta)}{f(\beta)g'(\beta) - g(\beta)f'(\beta)}\right] + \left[g(\alpha) - \frac{g'(\alpha)}{\mathrm{i}k_1}\right]\left[\frac{f'(\beta) - \mathrm{i}k_3 f(\beta)}{f'(\beta)g(\beta) - g'(\beta)f(\beta)}\right]\right\}, \tag{35c}$$

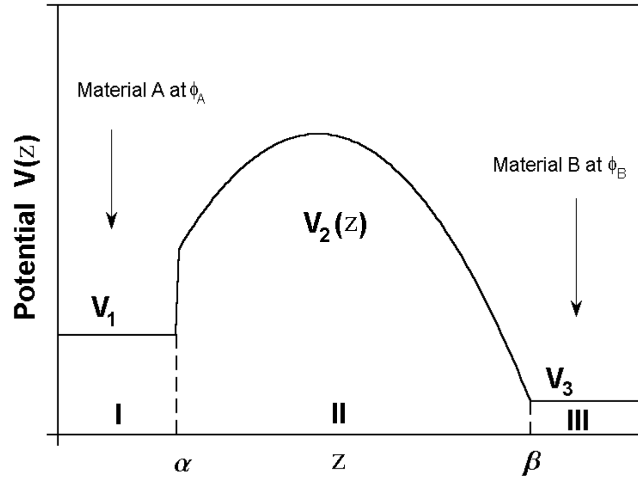

Figure 7. A general potential barrier system, with $V_2(z)$ for $\alpha < z < \beta$, sandwiched in between materials A and B at electrostatic potentials ϕ_A and ϕ_B. The particles are incident from the left.

where $k_i = \sqrt{2m(\varepsilon - V_i)/\hbar^2}$ and V_i is the potential associated with region i. The boundary matched normalized wavefunctions of equation (33) for each of the regions I, II and III are

$$\frac{\psi_I}{A_1} = \mathrm{e}^{\mathrm{i}k_1 z} + \frac{t_{21}}{t_{11}}\mathrm{e}^{-\mathrm{i}k_1 z}, \qquad z < \alpha, \tag{36a}$$

$$\frac{\psi_{II}}{A_1} = \frac{A_2}{A_1} f(z) + \frac{B_2}{A_1} g(z), \qquad \alpha \leqslant z \leqslant \beta \tag{36b}$$

and

$$\frac{\psi_{III}}{A_1} = \frac{1}{t_{11}}\mathrm{e}^{\mathrm{i}k_3 z}, \qquad z > \beta, \tag{36c}$$

where the energy-dependent coefficients are

$$\frac{A_2}{A_1} = \left[\frac{\mathrm{e}^{\mathrm{i}k_1\alpha}[g'(\alpha) - \mathrm{i}k_1 g(\alpha)] + \frac{t_{21}}{t_{11}}\mathrm{e}^{-\mathrm{i}k_1\alpha}[g'(\alpha) + \mathrm{i}k_1 g(\alpha)]}{f(\alpha)g'(\alpha) - f'(\alpha)g(\alpha)}\right], \tag{37a}$$

$$\frac{B_2}{A_1} = \left[\frac{\mathrm{e}^{\mathrm{i}k_1\alpha}[f'(\alpha) - \mathrm{i}k_1 f(\alpha)] + \frac{t_{21}}{t_{11}}\mathrm{e}^{-\mathrm{i}k_1\alpha}[f'(\alpha) + \mathrm{i}k_1 f(\alpha)]}{f'(\alpha)g(\alpha) - f(\alpha)g'(\alpha)}\right]. \tag{37b}$$

Finally, the values of the functions $f(z)$ and $g(z)$ and their derivatives at $z = \alpha, \beta$, associated with $V(z)$ of figure 7, are obtained numerically using a Runge–Kutta [96] scheme with appropriate initial guesses [94]. The effectiveness of this approach has been demonstrated previously [94] with the additional inclusion of a variable effective mass.

Also, since the full wavefunction must obey the Landau normalization rule [73] for the incident probability current, $A_1 = \frac{1}{\sqrt{2\pi\hbar}}$. In sections 3.2 and 3.3 we will refer to the above method along with the use of equation (27) as the non-self-consistent Landauer formula (NSLF) method.

It is possible to include self-consistency and the fact that the electronic effective mass varies as a function of z in a realistic potential barrier system. In this case equation (32) is replaced by the BenDaniel–Duke equation [97] in the z direction:

$$-\frac{\hbar^2}{2}\frac{\partial}{\partial z}\frac{1}{m(z)}\frac{\partial}{\partial z}\psi(\varepsilon, z) + [V_o(z) + V_e(z)]\psi(\varepsilon, z) = E\psi(\varepsilon, z). \tag{38}$$

Here, $V_o(z)$ is as before and $V_e(z)$ is the Hartree potential [98] that is obtained self-consistently. It represents the contribution to the potential due to the electron's motion in the field of other electrons and neglecting exchange–correlation contributions to the potential [99] which can, in principle, be included. The self-consistency is achieved through the above equation (38) and the Poisson equation:

$$\frac{\partial}{\partial z}\varepsilon(z)\frac{\partial}{\partial z}V_e(z) = -\rho(z), \tag{39a}$$

with a z-dependent dielectric. The charge density is written as

$$\rho(z) = e^2\left[\frac{N(z)}{A} + N_a^-(z) - N_d^+(z)\right]. \tag{39b}$$

Here, N_a^- and $N_d^+(z)$ are the ionized acceptor and donor volume concentrations. The electron concentration is written as

$$N(z) = \tfrac{1}{2}\int_0^\infty \mathrm{d}\varepsilon\,\{n_L(z,\varepsilon)F_L(z,\varepsilon)\psi_L(z,\varepsilon)\psi_L^*(z,\varepsilon) + n_R(z,\varepsilon)F_R(z,\varepsilon)\psi_R(z,\varepsilon)\psi_R^*(z,\varepsilon)\}, \tag{40}$$

where the left and right sides of the potential Fermi functions are written as

$$F_{L,R}(\varepsilon) = (1 + \exp[(\varepsilon - \mu_{L,R})\beta_T])^{-1}, \tag{41}$$

with the use of the structure's left and right side Fermi levels. The left Fermi level, μ_L, is obtained through the charge neutrality condition $\int_0^L \rho(z)\,\mathrm{d}z = 0$ for zero applied bias, where L is the total sample length. On the right side, we assume the form $\mu_R = \mu_L - e\varphi_{bias}(L)$, as in [100]. We refer to this, along with the use of equation (27), as the SLF.

The left and right wavefunctions, $\psi_L(\varepsilon, z)$ and $\psi_R(\varepsilon, z)$, of equation (40) are obtained as outlined above; however, in equation (34) we set $B_3 = 0$ for waves travelling rightward and set $A_1 = 0$ for waves travelling leftward. In equation (40) we made use of the 2d density of states [24], so that $n_L = n_R = Am^*/\pi\hbar^2$, where m^* is the GaAs effective mass, consistent with the structure of interest here. Further, the ionized donor and acceptor temperature-dependent concentrations are to be used in equation (39b) as given by [83]

$$N_d^+ = \frac{N_D}{1 + 2\mathrm{e}^{-(\varepsilon_D - \mu_L)\beta}}, \qquad N_a^- = \frac{N_D}{1 + 2\mathrm{e}^{-(\varepsilon_A - \mu_L)\beta}}, \tag{42}$$

with $\varepsilon_{A,D}$ the acceptor and donor binding energies. The self-consistency in the Hartree potential $V_e(z)$ is achieved by first obtaining an initial trial wavefunction with $V_e(z) = 0$. The wavefunction is substituted into equations (39) and (40), so that the Poisson equation is solved with $V_e(0) = 0$ and $V_e(L) = -e\phi_{bias}(L)$ boundary conditions, where $\phi_{bias}(z) = Ez$ and E is the applied electric field. The resulting potential is used in equation (38) which in turn gives a new wavefunction. The process is repeated until the change in $V_e(z)$ is less than about 0.5 meV. Once the final Hartree potential is obtained, $V(Z) = V_o(z) + V_e(z)$ is used in equation (35) to obtain the transmission coefficient corresponding to the SLF, with the current calculated by the LF, equation (27). In the NSLF $V_e(z)$ is taken to be zero and the transmission coefficient is effected from the start using equations (35) and (27) only. Thus, the SLF differs from the NSLF by the presence of the Hartree potential $V_e(z)$. Below, both methods are included in order to provide a comparison with the work of [63]. Further, a comparison is also included between the current obtained through the LF and the current obtained through the use of the STT.

3.2. Application to double-barrier (single well) system

We work with dimensionless units: energy is given in units of $\varepsilon_b = me^4/[2\hbar^2(4\pi\varepsilon_0 K_{\mathrm{GaAs}})^2] =$ 5.247 meV, distance is in units of a_b, where $a_b \equiv k_b^{-1} = \sqrt{\hbar^2/2m\varepsilon_b} = 101.9$ Å, with the gallium arsenide's dielectric constant, $K_{\mathrm{GaAs}} = 13.18$, and effective mass, $m* = 0.067\ m_e$, where m_e is the mass of a free electron. The electric field has units of $E_{elb} = \varepsilon_b/ea_b =$ 5.04 kV cm^{-1} and the unit of temperature is $T_b = \varepsilon_b/K_B = 60.897$ K. The conductance unit is $G_b = e^2/\hbar = 2.43 \times 10^{-4}$ ℧. The electrostatic potential difference between the A and B sides of the sample is $\Delta\phi = E\ell$ in units of $\phi_b = E_{elb}a_b$ with ℓ being the distance between the α and β points in figure 7. The double-barrier potential, $V(z)$, of figure 7 takes the form

$$V(z) = \begin{cases} V_1 & \text{for } z < \alpha \\ V_2 - (z-\alpha)E & \text{for } \alpha < z < \alpha + w_1 \\ V_3 - (z-\alpha)E & \text{for } \alpha + w_1 < z < \alpha + w_1 + w_2 \\ V_2 - (z-\alpha)E & \text{for } \alpha + w1 + w_2 < z < \alpha + w_1 + w_2 + w_3 \\ V_3 - (\beta-\alpha)E & \text{for } z \geqslant \alpha + w_1 + w_2 + w_3, \end{cases}$$

with $\alpha = -3a_b$, $\beta = \alpha + w_1 + w_2 + w_3$. Below, first we use the NSLF method and take the barrier widths $w_1 = w_3$, then we vary their size. We also take $V_1 = V_3 = 0$ and vary the barrier height V_2 as well as the width w_2. Figure 8 shows the case of $V_2 = 1\varepsilon_b$, $w_1 = 3a_b = w_2$, $E_F = 3\varepsilon_b$. Below the calculations are for the average conductance and from here on this is referred to just as conductance. The obtained conductance, versus the electric field, using equations (5) and (27), at 10 K is shown in figure 8(a). It reaches a maximum at $E = 0.2125E_{elb}$ and decays as the field is increased. We show the potential $V(z)$ for various values of the electric field in figure 8(b). In figure 8(c), the Fermi function difference, $F_A(\varepsilon) - F_B(\varepsilon)$, which plays an important role in equation (27) is shown for four field values, including the field value at which the conductance of figure 8(a) peaks. In figure 8(d) we show the transmission coefficient corresponding to the potential cases shown in figure 8(b). We see, first of all, that at $E = 0.0625E_{elb}$ there is a resonant level and a Ramsauer type of resonance in figure 8(d). At this value of the field, however, the conductance is increasing due to the high overlap between $F_A - F_B$ at the high energy part of the transmission. As the field increases to $E = 0.2125E_{elb}$, the function $F_A - F_B$ overlaps more of the transmission spectrum, causing the conductance to reach its maximum value. Beyond this field value, the conductance does not experience an extra appreciable contribution since $F_A - F_B$ no longer broadens and begins to remain constant. The transmission coefficient increases: however, the conductance begins to decrease as $1/E$, as mentioned earlier.

Based on the results of figures 8, we should expect more interesting behaviour as the levels in the well are increased accompanied by a decrease in the barrier widths. This is indeed the case as shown in figures 9. Here, we let $w_1 = 1a_b$, $V_2 = 3\varepsilon_b = E_F$ and we let the electric field vary as $E = [0.4/(\beta - \alpha)]E_{elb}$. Also, the well width takes on the values $w_2 = 3$, 5 and 10 in units of a_b. The potential plots are shown in figure 9(a) with corresponding transmission coefficients in figure 9(b). The wells support 2, 3 and 5 levels, respectively. The conductance for each potential case is given in figure 9(c). As the well width becomes greater, we see that the conductance peak shifts to a lower field due to the increased number of level resonances in the transmission. In particular, the case of $w_2 = 10a_b$ experiences further structure. As expected, the Fermi function difference, $F_A - F_B$, obtains a high overlap with the highest energy level in the well at the corresponding value of electric field for the first conductance peak. The dip that occurs at a slightly higher field is due to no appreciable further increase in the overlap between $F_A - F_B$ and $T(\varepsilon)$ for this field value. However, as the field is increased, we can see a second peak, in figure 9(c) for $w_2 = 10a_b$, which is due to the strong overlap

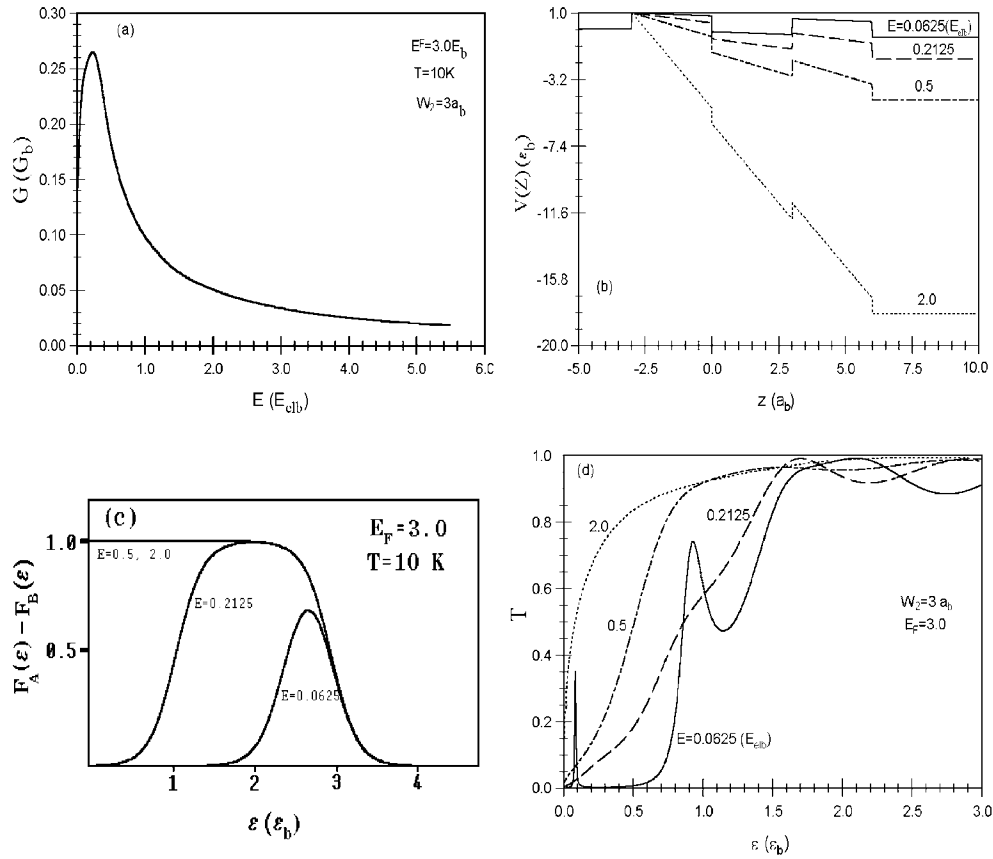

Figure 8. Calculations for a double-barrier system with $V_2 = 1\varepsilon_b$, $w_1 = w_3 = w_2 = 3a_b$, $E_F = 3\varepsilon_b$. (a) The average conductance in units of G_b versus the electric field in units of E_{elb} at 10 K. (b) The potential $V(z)$ versus z for field values of 0.0625, 0.2125, 0.5 and 2.0 E_{elb}. (c) The Fermi function difference F_A–F_B versus ε (ε_b) for field values of figure 8(b). (d) The transmission coefficient versus ε (ε_b) for the field values of figure 8(b).

between $F_A - F_B$ and two large contributions of $T(\varepsilon)$, due to two levels for this wide well case. This is expected because, as E is increased, $F_A - F_B$ broadens as explained before in figure 8(c). With a further field increase, the conductance tends to decay as $1/E$ and this factor wins out over any further increase in overlap contribution due to the fact that $T(\varepsilon)$ changes with electric field. At much higher field, the well no longer supports energy levels; however, Ramsauer oscillations continue to play a role and this is the reason for slight deviations from the $1/E$ behaviour in the conductance.

It appears that, while the conductance should decrease in temperature, it should still give evidence of interesting structure versus field, especially for wide wells and low field in a similar way as shown for the $T = 10$ K case. This is indeed the case, as can be seen in figure 10, where the $T = 77$ and 300 K conductances, for the $w_2 = 10a_b$ well, are compared with the 10 K result. While the conductances do decay with E and T, we see that a structure does appear. At higher temperature, there seem to be more oscillations because the $F_A - F_B$ function difference is rather broad and encompasses a large overlap with the $T(\varepsilon)$ spectrum; nevertheless, the oscillations are not strong due to the $1/T$ dependence of the conductance.

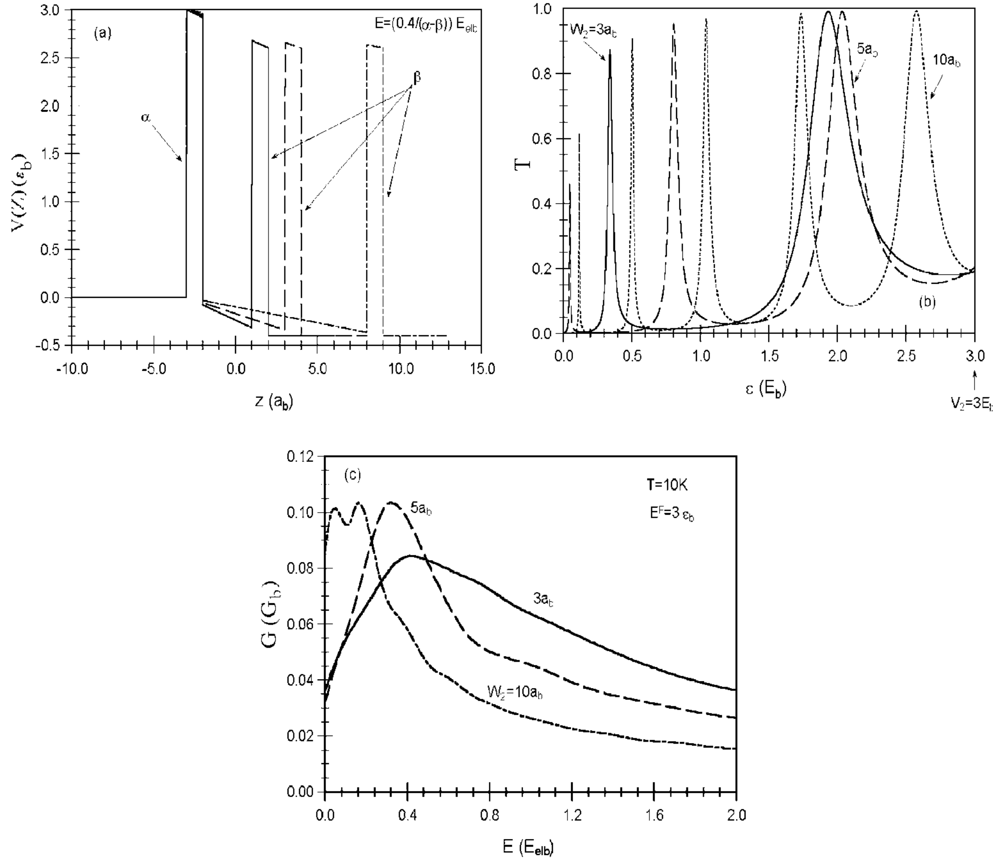

Figure 9. Calculations for a double-barrier system at 10 K with $w_1 = w_3 = 1a_b$, $V_2 = 3\varepsilon_b = E_F$ and an electric field that varies as $E = 0.4/(\beta - \alpha)$ in units of E_{elb}, where α and β are the left and right edges of the potential barrier. Here the well widths used are $w_2 = 3$, 5 and $10a_b$. (a) The potential versus z (a_b) for each of the three well widths. (b) The transmission coefficient versus ε (ε_b) for each of the three well widths. (c) The average conductance in units of G_b versus the electric field in units of E_{elb} for each of the three well widths.

We next work with the specific, but more realistic, potential of [63]; accordingly, the following parameters are used: $N_A \equiv 0$, $N_D = 2 \times 10^{24}$ m^{-3}, $E_D = 16.4\varepsilon_b$, $V_1 = 0.0$, $V_2 = 0.27$ eV, $V_3 = V_1$, $\alpha = 175$ Å, $w_1 = 28$ Å, $w_2 = 45$ Å, $w_3 = w_1$, $\beta = 276$ Å. The GaAs regions (V_1) lie between $0 < z < \alpha$, $\alpha + w_1 < z < \alpha + w_1 + w_2$ and $\beta < z < L$, where $L = \beta + \alpha$. The $Al_{0.3}Ga_{0.7}As$ barrier (V_2) regions exist for $\alpha < z < \alpha + w_1$ and $\alpha + w_1 + w_2 < z < \beta$. The effective mass and dielectric constants for the material compounds used are $m_{\mathrm{GaAs}} = 0.067\, m_e$, $m_{\mathrm{AlAs}} = 0.15\, m_e$, $K_{\mathrm{GaAs}} = 13.18$, $K_{\mathrm{AlAs}} = 10.06$. In the case of $Al_xGa_{1-x}As$, the corresponding value of effective mass and dielectric constant is obtained by a linear combination of the compound parameters with concentration x for AlAs using a virtual crystal approximation [101]. Finally, the self-consistently obtained Fermi levels for temperatures of 10, 77 and 300 K are $\mu = 16.383$, 16.278 and 15.976 in units of ε_b, respectively.

In figure 11(a), the result obtained for the self-consistent electron charge distribution in units of a_b^{-3}, equation (40), versus z in units of a_b, for voltage values of 0.1, 4.5 and 50.5 in units of ϕ_b, and a temperature of 300 K is shown. We see here that, as the field

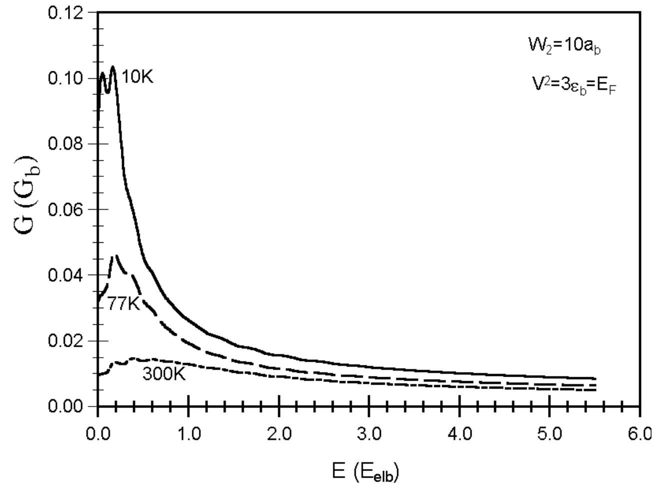

Figure 10. The average conductance (G_b) versus E (E_{elb}) calculations for a double-barrier system of $w_2 = 10a_b$ at $T = 10$, 77, and 300 K. The rest of the parameters are as in figure 9.

is increased, the charge gets depleted, as z increases, from the system as indicated by the variation versus field. It is interesting to note that the conductance is correspondingly lower for the higher field value as will be seen in figure 11(c). In figure 11(b), the full potential, $V(z) = V_o(z) + V_e(z)$ in units of ε_b, which includes the self-consistently obtained Hartree contribution, is plotted versus z (a_b) for two values of the voltage, $4.5\phi_b$ and $50.5\phi_b$, at 300 K (the non-self-consistent case is shown as a broken line). Here the self-consistent Hartree contribution tends to make the potential vary in a nonlinear fashion, in contrast to the linear behaviour of simply superimposing an electrostatic potential due to a constant electric field. The Hartree term causes the transmission coefficient to change dramatically versus energy compared to the case of the NSLF. In figure 11(c), we compare the conductance in units of G_b versus electric field (E_{elb}) for three methods at 77(300) K, i.e. the NSLF 1(4), the SLF 2(5) and the STT 3(6) mentioned in the previous section. The STT and the NSLF are closer to each other at high temperature, but at low temperature there is more contrast between them. The reason is that the STT has a small temperature dependence. The NSLF and the SLF both show a moderate temperature dependence marked by the increase in conductance at low temperatures. This is consistent with our earlier discussion in figures 7–9. The STT, however, shows a slightly higher conductance at higher temperature. This behaviour contrasts with that of the Landauer approaches and is attributed to the difference in the way each weighs the transmission coefficient in calculating the current as discussed in section 2. This trend continues for lower temperature. The main difference between the SLF and the NSLF is that, because of the self-consistent Hartree potential contribution, the SLF shows a peaking of the conductance that is different from the way the NSLF behaves at low field. For this particular system, there is a level in the well at about $18\varepsilon_b$. This level moves down as the electric field is increased. In the SLF, the level moves down much faster with the electric field than it does for the NSLF. Further, the conductance is higher at higher fields in the SLF, due to a consistent contribution to the transmission coefficient from the Ramsauer-like resonances, than in the NSLF. At very high fields both conductances begin to drop again, however, as expected in our earlier discussion.

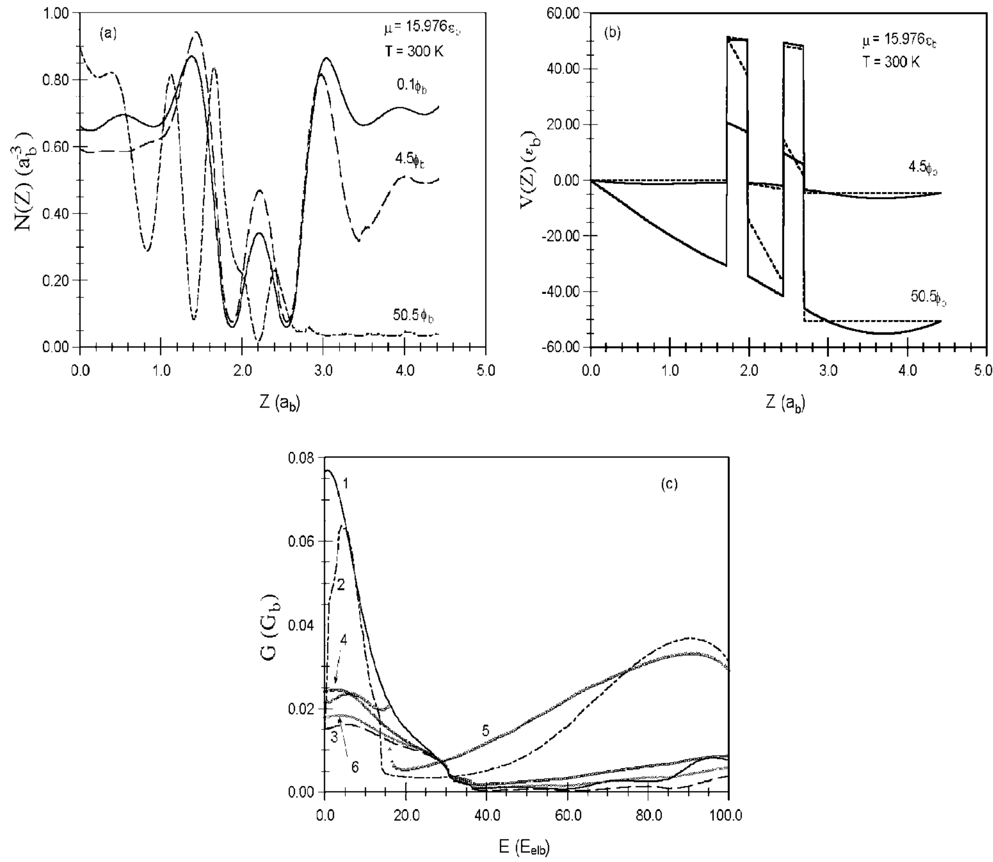

Figure 11. Calculations for a realistic structure potential of AlGaAs of [63]. (a) The self-consistent electronic charge distribution in units of a_b^{-3} versus z in units of a_b, for bias voltage values of 0.1, 4.5 and 50.5 in units of ϕ_b at 300 K. (b) The full potential, $V(z) = V_o(z) + V_e(z)$, in units of ε_b, which includes the self-consistently obtained Hartree contribution, versus $z(a_b)$ for two values of the voltage $4.5\phi_b$ and $50.5\phi_b$ at 300 K (the non-self-consistent case is shown as a broken curve). (c) The average conductance in units of G_b versus electric field (E_{elb}) for three methods at 77(300) K, i.e. the NSLF 1(4), the SLF 2(5) and the STT 3(6).

Finally, a comparison between the Landauer approach and the Wigner function distribution scheme of [63] in figure 12. The figure shows a comparison for the current density versus bias voltage for a GaAs/$Al_{0.3}Ga_{0.7}As$ double-barrier system. We use the potential parameters of [63] as mentioned above. For comparison purposes we use the doping density of the GaAs well, 2×10^{18} cm^{-3}, to get an electron well areal concentration of $N_s = 9 \times 10^{11}$ cm^{-2}. Figure 12 shows [63]'s current density results for their Wigner distribution function schemes, UDS-3 (filled circles) and UDS-4 (open circles), corresponding to variable and constant effective masses. The Landauer current density results, for the SLF 1(3) and the NSLF 2(4) at $T = 10(300)$ K, using equation (27) with $J = N_s I$, which include the position-dependent effective mass, are shown. Our current densities increase initially versus voltage due to a resonant level ($\sim$99 meV) contribution in $T(\varepsilon)$ which lies above the Fermi level (86.4 meV) at zero field, but moves down and below the Fermi level at higher field. For the field value corresponding to about 0.8 V, the level is below zero in the SLF so that its current experiences a sudden drop for both temperatures. The NSLF, however, continues to get a current contribution

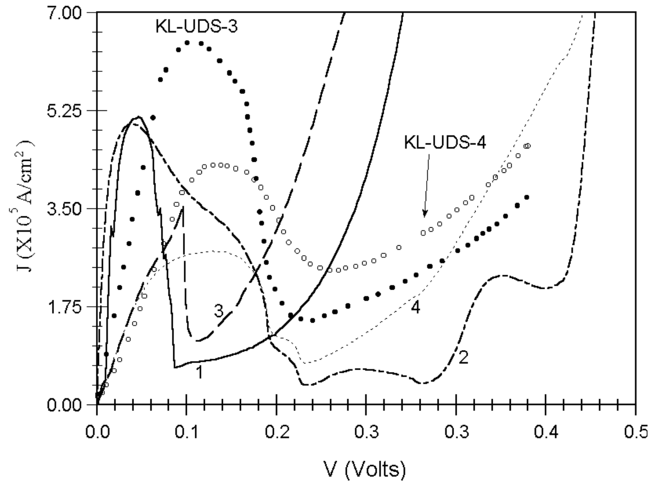

Figure 12. The current density versus voltage for the potential of [63] at $T = 10$ and 300 K. The curves labelled 1, 2, 3 and 4 are our LF results at 10(300) K for the SLF 1(3) and the NSLF 2(4). The Wigner function schemes, labelled KL-UDS-3 (filled circles) and KL-UDS-4 (open circles) of [63] are shown for comparison.

from the level because its potential does not include the Hartree field. As the voltage increases, current density begins to increase again due to Ramsauer resonances playing a strong role in $T(\varepsilon)$ at energy values below the Fermi level, with the NSLF showing more structure due to its different potential form. This is not surprising in view of our previous discussion. The comparison is rather interesting since the Landauer calculations are less time consuming. We do note that the Wigner function results are very different, particularly in magnitude and shape. In the case of the LF approaches here, i.e. the SLF (curves 1, 3) and the NSLF (curves 2, 4), the decrease in current density for higher temperature is expected as discussed in figure 10 for low field values. We also note that the Wigner distribution function result is probably not sensitive to variations in the details of the transmission coefficient as in the LF cases. This is the main reason for the difference in the current comparison. Finally, note the shift in current maximum with higher temperature in the LF approaches. This is due to the broadening in the Fermi distribution function.

3.3. Application to the triple-barrier (double well) system

The first evidence of tunnelling between two purely 2D systems separated by a single barrier was reported in the late 1980s [102]. The early work of Zohta *et al* [32], for a triple-barrier system, demonstrated the significance of tailoring a barrier that would separate electrons in two different quantum wells. Interesting I–V characteristics were observed in that work [32] including NDR properties and high peak to valley ratios. Here, the numerical approach of the previous subsection is applied to the triple-barrier system shown in figure 13. Figure 13(a) shows the effect of varying the middle barrier height. In this example the potential used is such that there are three barriers and two wells. The end barriers have a fixed height of $1\varepsilon_b$ and the middle barrier is shown to change from zero to $2\varepsilon_b$ in steps of $1\varepsilon_b$ in order to see the effect on the wavefunction and later the conductance. The barriers use a width of $1\varepsilon_b$ and the wells have a width of $3.5\varepsilon_b$. The Fermi level is at about $0.9\varepsilon_b$. Since samples have conducting contacts beyond the end barriers, the electron wavefunction is free, which is not shown in the figure.

The effect of the middle barrier is to raise the energy of the resonant states, as can be seen in figure 13(a). In addition, the higher the middle barrier is, the smaller is the overlap between the two wells as expected. In figure 13(b) for an applied field of $0.4E_{elb}$, one sees that the smaller and no middle barrier cases involve free motion. The case of the $2\varepsilon_b$ barrier, however, does have a resonant state, but the wavefunction has a free electron shape due to resonant tunnelling at this field value. The effect of the middle barrier height on the transmission coefficient is shown in figure 14. As the electric field is increased from zero in figure 14(a) through $0.4E_{elb}$ in figure 14(b) to $0.6E_{elb}$ in figure 14(c), the transmission coefficient experiences a higher contribution due to resonance, but experiences the least contribution at off resonance as shown in figure 14(c). This in essence demonstrates the significance of the middle barrier. In fact, figure 15 shows clearly the effect discussed earlier [32], i.e. the conductance experiences a double peak value as calculated using both the LF and the STT methods. The STT seems to have a smaller magnitude. The reason the double well, triple-barrier, system has high peak to valley conductance is due to the special resonance condition associated with the middle barrier, as mentioned in figure 14. At the appropriate field value, the middle barrier contributes to resonant tunnelling, but at an off-resonant field it actually scatters the electron wavefunction and causes the conductance to drop. Figure 15 demonstrates the tailoring of the middle barrier. The double peak is due to the fact that, as the field is much higher, the middle barrier tends not to affect the conductance any further so it is closer to the value without a middle barrier. Figure 16 shows the effect of including the Hartree term and self-consistency to the double well potential. The self-consistency tends to lift the middle barrier as shown in figure 16(a) for the voltage values of 0.1, 1 and $4.5\phi_b$. The corresponding electron charge distribution for this system is shown in figure 16(b) which also includes a higher field value curve. The shape of the charge distribution for this system is to be contrasted to those of the double-barrier system (figure 11(a)). Finally, the SLF conductance is shown in figure 17. The shapes are similar to the NSLF ones of figure 15 but shifted slightly higher in energy due to the contribution from the Hartree potential.

4. Inclusion of the magnetic field

The tunnelling experiments of Smoliner *et al* [102], where electrons tunnel from a TEG well to another, provided the means to investigate the effect of superimposing a magnetic field on a structure [103, 104]. The magnetic field direction has a dramatic effect on the tunnelling current. In the case of a field applied in the z direction or parallel to the tunnelling current, that is, perpendicular to the interfaces, has the effect of quantizing the electron motion in the x, y planes giving rise to Landau levels. Early evidence of such effect was demonstrated for the case of GaAlAs–GaAs–GaAlAs heterostructures [105] and reported later for GaAs/GaAlAs double well systems [103]. Applying a magnetic field in the direction parallel to the interfaces, that is, perpendicular to the tunnelling direction, has the effect of significantly changing the I–V characteristics, such as, for example, shifting the NDR region to higher voltages [104, 105] and broadening the resonant peaks [106]. In both magnetic field configurations, energy and momentum conservation play an important role in the I–V characteristics [105, 107].

4.1. Magnetic field in the direction of the tunnelling current

Starting from a general form of a one-electron Hamiltonian in the presence of a magnetic field and a confining potential in the z direction, ignoring spin,

$$H = \frac{1}{2m}(\vec{p} + e\vec{A})^2 + V(z), \tag{43}$$

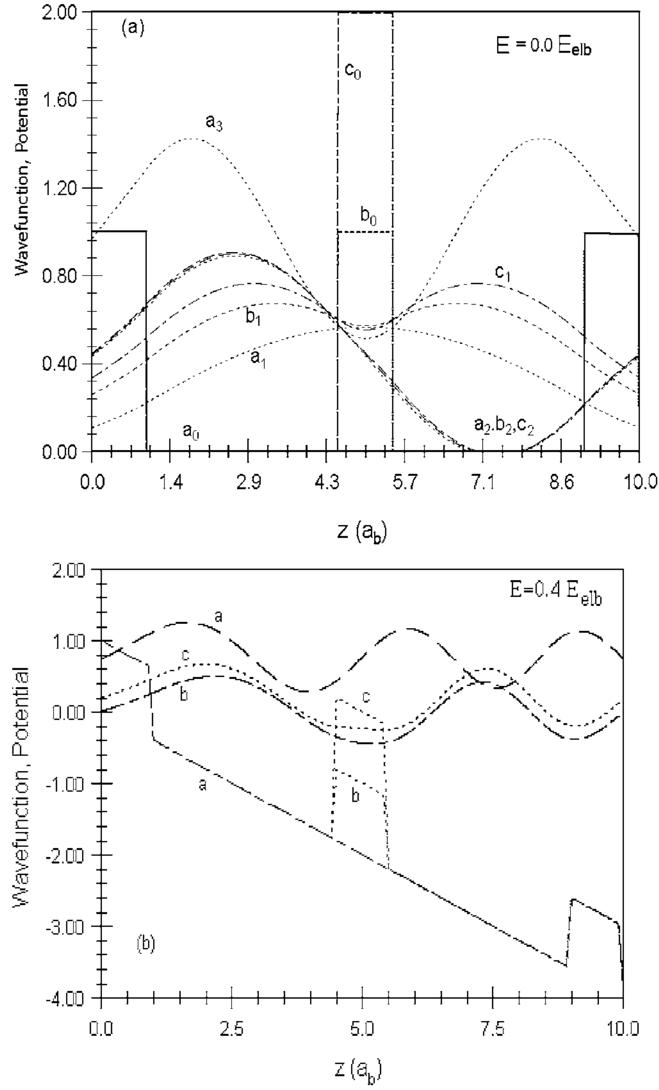

Figure 13. Double well potential system with middle barrier. (a) States shown are for (curve a) zero ε_b, (curve b) one ε_b and (curve c) two ε_b heights of two states (1, 2). The second state is similar for all three barrier sizes. (b) As in (a) for a field value of $0.4E_{elb}$. The higher barrier state (curve c) is a resonant level on the first well.

and specializing to a magnetic field parallel to the tunnelling current, $\vec{B} = B_z\hat{k}$, with the vector potential given by, $\vec{A} = A_y\hat{j}$, where $A_y = B_z x$, i.e. the Landau gauge [73], as can be checked by $\vec{B} = \vec{\nabla} \times \vec{A}$, the Hamiltonian becomes

$$H = \frac{1}{2m}[p_x^2 + (p_y + eB_y x)^2 + p_z^2] + V(z). \tag{44}$$

This corresponds to free electron motion in the y direction, harmonic motion in the x direction and confined motion in the z direction. In fact, if we assume a solution to the Schrödinger

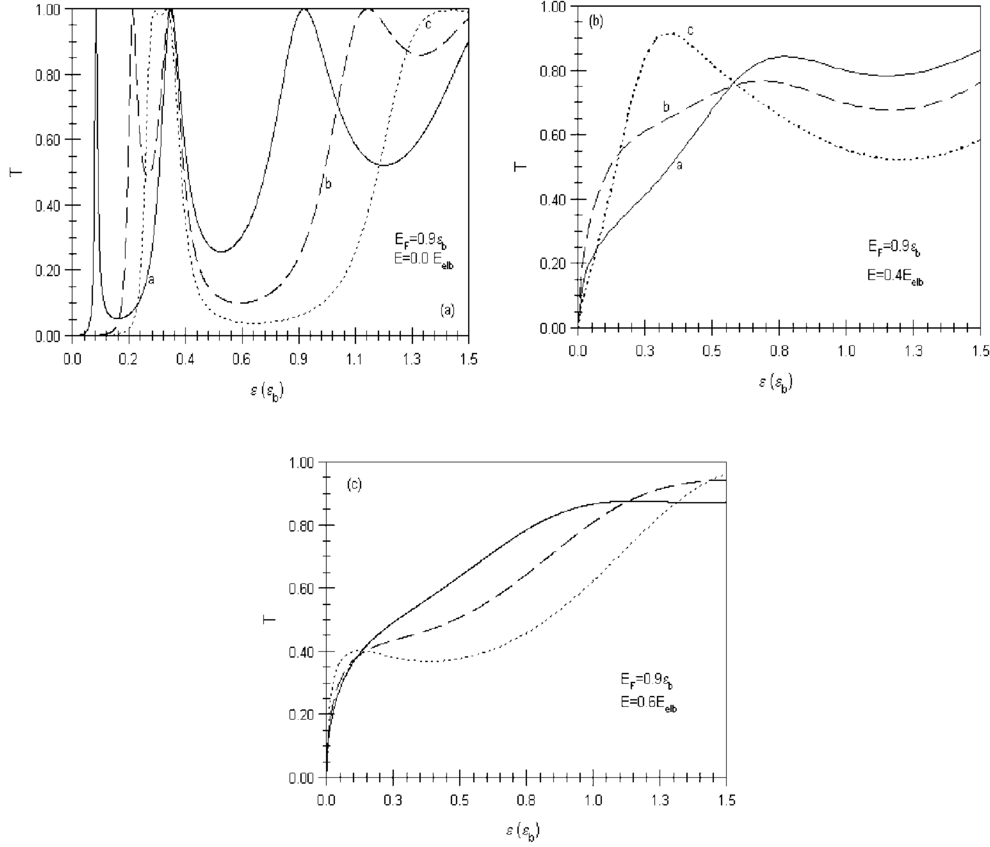

Figure 14. (a) Transmission at zero field for middle barrier cases of $0\varepsilon_b$, $1\varepsilon_b$ and $2\varepsilon_b$. (b) As in (a) for a field value of $0.4E_{elb}$. (c) As in (a) for a field value of $0.6E_{elb}$.

equation, $H\psi = \varepsilon\psi$, in the form

$$\psi = f(z)g(x)\exp(\mathrm{i}k_y y) \tag{45}$$

we find the differential equations obeyed by $g(x)$ and $f(z)$ in the form

$$-\frac{\hbar^2}{2m}\left[\frac{\partial^2}{\partial x^2} - \left(k_y + \frac{eB_z x}{\hbar}\right)^2\right]g(x) = \varepsilon_N g(x), \tag{46a}$$

$$-\frac{\hbar^2}{2m}\left[\frac{\partial^2}{\partial z^2} + V(z)\right]f(z) = \varepsilon_n f(z), \tag{46b}$$

where the total energy is given by $\varepsilon(n, N) = \varepsilon_n + \varepsilon_N$. The functions $g(x)$ are the standard harmonic oscillator wavefunctions [73] in the x direction whose centre of motion depends on the momentum in the y direction, $-k_y$. The eigenvalues $\varepsilon_N = (N + \frac{1}{2})\hbar\omega_c$ with $\omega_c = eB_z/m$ are the Landau levels mentioned before. In the z direction, the shape of $f(z)$ depends on the confining potential $V(z)$. For resonant states in a quantum well, such as, for example, a double-barrier structure of section 3, the functions $f(z)$ can be obtained numerically and the resonant energies ε_n generated. Thus, for the present magnetic field configuration, under an additional applied voltage, as in section 3, the resonant tunnelling condition is shifted by a magnetic field dependent energy. The resonant tunnelling discussed previously in section 3

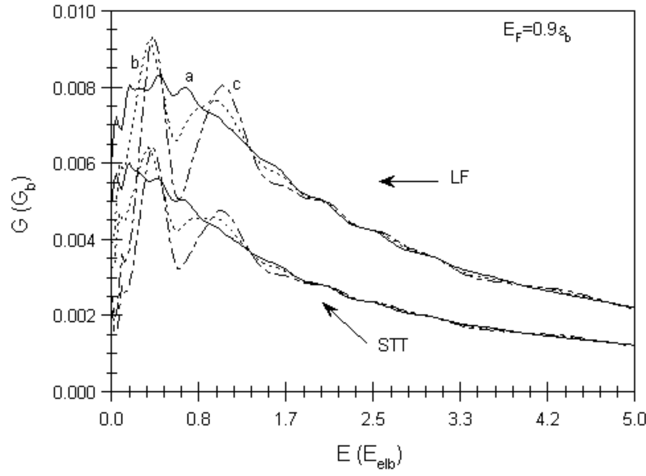

Figure 15. Average conductance (G_b) for the three barrier cases of figures 13 versus field. The STT curves are lower in magnitude than the NSLF. Curves a, b and c correspond to the three potentials of figure 13.

now becomes $E_F + e\Delta\phi = \varepsilon(n, N)$. In analogy to the $B = 0$ case, resonant tunnelling does not occur for a voltage below a value $\Delta\phi_1$. In addition, resonant tunnelling does not occur beyond a second voltage $\Delta\phi_2$ because of the shape of the density of states, which is peaked around a given Landau level. Instead the voltage would need to be increased further in order to get additional resonant tunnelling from a higher Landau level. The I–V shape of the double-barrier system develops an oscillatory character as shown in figure 18 [105], referred to as resonant magneto-tunnelling. Not surprisingly, a similar oscillatory behaviour is found in the double well one-barrier system of Smoliner *et al* [103] where each well supports its own set of Landau levels. The transitions obtained by the authors between different Landau levels versus applied voltage is shown in figure 19 [103], where, in the absence of scattering due to energy and momentum conservation, the applied voltage adjusts the subbands of each well energetically according to the resonance condition $\varepsilon_1(n, N) = \varepsilon_2(m, N)$, for wells 1 and 2, respectively, assuming $k_\parallel(k_x, k_y)$ is conserved which is responsible for the Landau level index conservation. For fields higher than about 5 T, however, complications in the experimental data arise due to the occurrence of a Hall voltage, in addition to impurity and surface roughness scattering mechanisms which make transitions possible between Landau levels of different indices [108].

4.2. Magnetic field in the plane of the layers

In an extension of their earlier work [35] on tunnelling conductance in a system with two GaAs wells separated by a AlAs barrier, Eisenstein *et al* [93] performed similar studies between the two wells as a function of an applied magnetic field parallel to the 2D planes. The conductance was measured without an applied bias. Their results are shown in figure 20. According to their simple model [93, 109], as the magnetic field increases the conductance experiences changes in behaviour depending on the overlap of each well's Fermi surface. To first order in perturbation theory, the energies associated with each well are written as [93]

$$\varepsilon_1 = E_{0,1} + \hbar^2(k_x^2 + k_y^2)/2m, \tag{47a}$$

$$\varepsilon_1 = E_{0,2} + \hbar^2((k_x - k_B)^2 + k_y^2)/2m, \tag{47b}$$

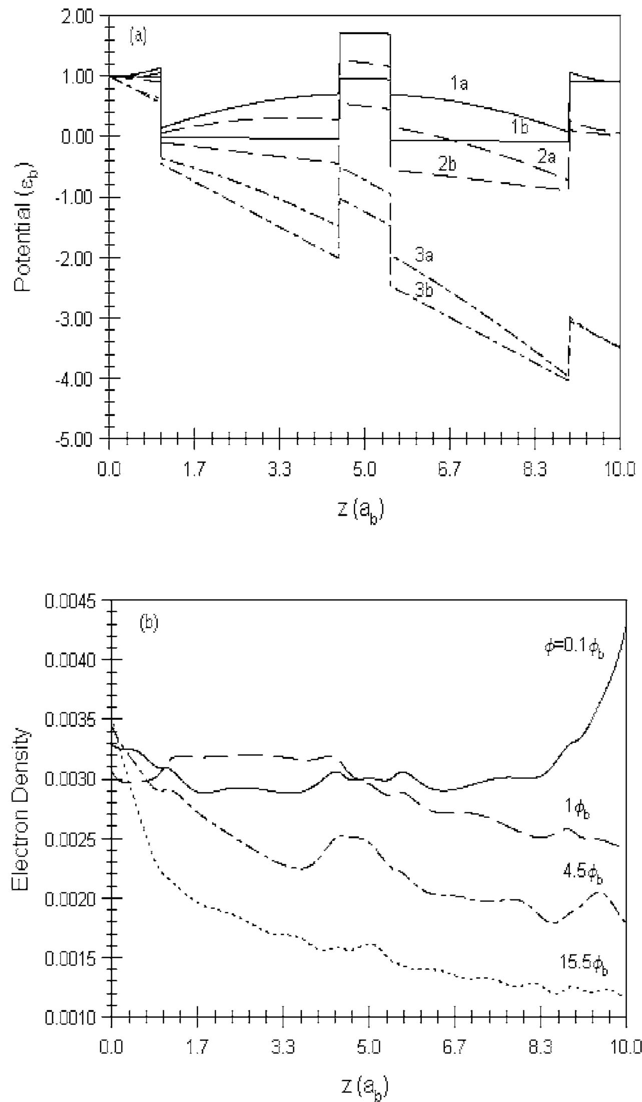

Figure 16. (a) The double-barrier potential with and without the self-consistent Hartree contribution for voltage values of 0.1, 1.0 and 4.5 in units of ϕ_b. (b) Electron charge distribution versus position for various field values and middle barrier of $1\varepsilon_b$ in the self-consistent calculation.

where $k_B = eBd/\hbar$ with d the separation between the wells and B the magnetic field in the y direction parallel to the well planes. When the magnetic field has zero value, tunnelling with energy and momentum conservation occurs when $E_{0,1} = E_{0,2}$, i.e. the ground state quantum energies due to the z direction confinement match. Increasing the magnetic field changes the position of the Fermi surface of the second well, with respect to the first, which is centred at $k_x = k_B$ whose radii are determined by the electron populations N_1 and N_2; thus tunnelling with conserved energy and momentum occurs only at the intersection of these circles, as shown in figure 20 [93]. A more complete picture can be obtained by considering a confined TEG, as in the previous subsection, but with a magnetic field in the x direction as in the work of

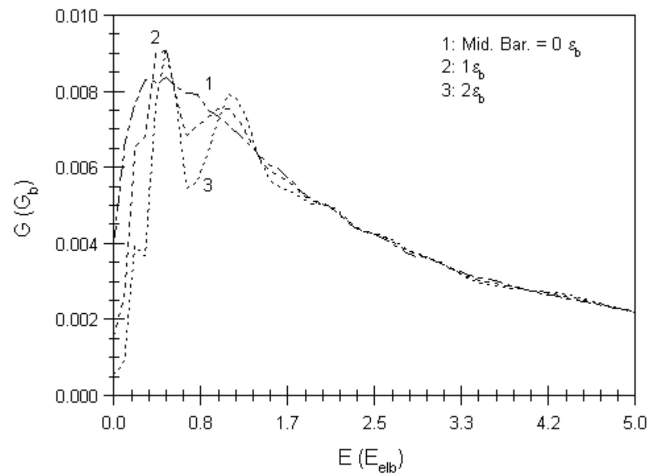

Figure 17. Self-consistent average conductance (G_b) using the LF versus electric field (E_{elb}).

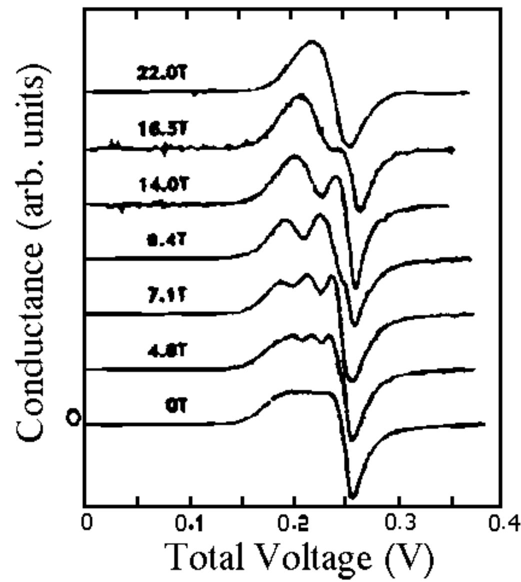

Figure 18. Conductance versus total voltage applied to sample A (see [105]) for various magnetic fields. The voltage drop between an electrode and the centre of the quantum well is half of the total voltage. The traces shown were taken at 0.55 K but no difference was found with data taken at 4.2 K [105]. Copyright (1986) by the American Physical Society. Reprinted with permission of APS and the authors.

Demmerle *et al* [108]. The Hamiltonian of this system is given by

$$H = \frac{1}{2m}[p_x^2 + (p_y - eB_x z)^2 + p_z^2] + V(z). \tag{48}$$

If we choose a wavefunction of the form $\psi = f(z)\exp(\mathrm{i}k_y y)\exp(\mathrm{i}k_x x)$, the Schrödinger equation results in a differential equation for the function $f(z)$ given by

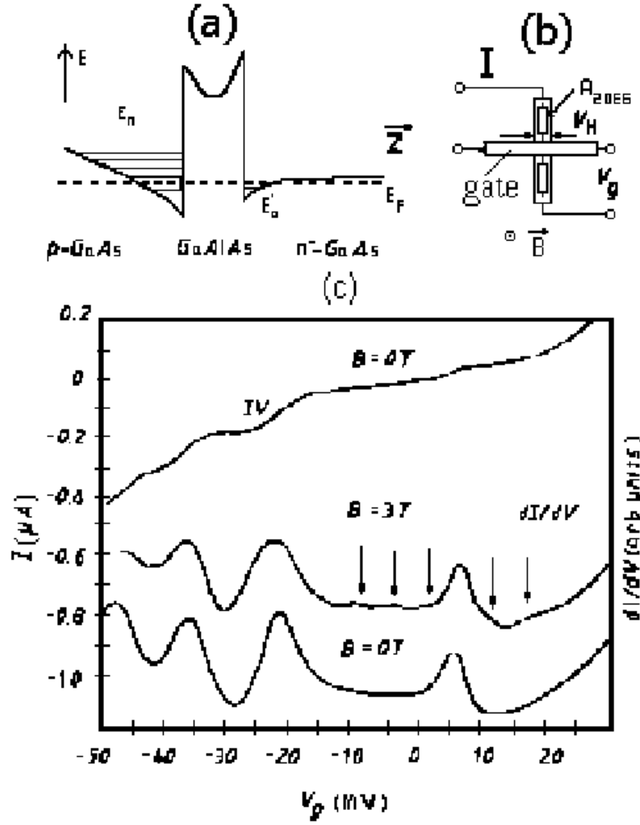

Figure 19. (a) Band structure of typical samples. E_n and E'_0 are the subbands in the inversion layer and the accumulation layer, E_F is the Fermi level. (b) Schematic figure of the sample geometry. I is the tunnelling current and V_g is the corresponding gate voltage. $R_{2D\ EG}$ represents the series resistance in the inversion layer and V_H is the Hall voltage at the gate contact. (c) I–V and $\mathrm{d}I/\mathrm{d}V$ curves for one typical sample (no 1816/13). The magnetic-field-induced structure in $\mathrm{d}I/\mathrm{d}V$ is indicated by arrows [103]. Copyright (1989) by the American Physical Society. Reprinted with permission of APS and the authors.

$$-\frac{\hbar^2}{2m}\frac{\partial^2}{\partial z^2}f(z)+\left[\frac{e^2B_x^2}{2m}(z-z_0)^2+V(z)\right]f(z)=\varepsilon_n(B_x,k_y)f(z), \tag{49}$$

where the total electron energy from $H\psi = \varepsilon\psi$ is written as

$$\varepsilon_{n,B_x,k_y,k_x}=\varepsilon_{k_x}+\varepsilon_n(B_x,k_y), \tag{50}$$

with $\varepsilon_{k_x}=\hbar^2k_x^2/2m$ and $z_0=\hbar k_y/eB_x$. It can be seen that the presence of the magnetic field in the plane of the layer (perpendicular to the tunnelling current) has the effect of adding a shifted parabolic potential to the original confining potential $V(z)$ whose curvature depends on the value of the field B_x [110]. It is possible to write the eigenvalues in equation (49) to lowest order in perturbation theory in the form

$$\varepsilon_n(B_x,k_y)\simeq-\frac{\hbar^2}{2m}\left\langle\frac{\partial^2}{\partial z^2}\right\rangle_0+\frac{e^2B_x^2}{2m}(\langle z\rangle_0-z_0)^2+\langle V(z)\rangle+\frac{e^2B_x^2}{2m}(\langle z^2\rangle_0-\langle z\rangle_0^2), \tag{51}$$

where $\langle\cdots\rangle_0$ refers to the average value carried out with the unperturbed z-dependent envelope function $f_0(z)$ in the absence of a magnetic field. If one neglects the last term, known as the

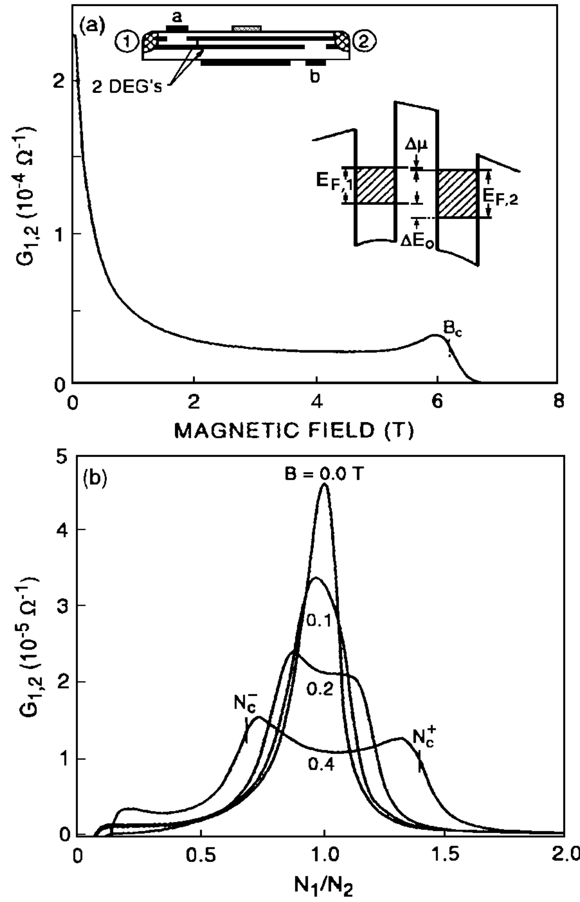

Figure 20. (a) Tunnel conductance versus magnetic field at $T = 0$ K. The 2d densities are 1.5 and 1.58×10^{11} cm^{-2} for the upper and lower quantum wells, respectively. The calculated critical field is indicated. Insets depict an idealized cross section through sample, showing ohmic contacts (hatched) and gate (shaded) and a schematic conduction-band diagram of the DQW. (b) Tunnel conductance versus ratio of upper to lower 2DEG densities at $T = 1.3$ K for several magnetic fields. Lower 2DEG density is fixed at about 0.90×10^{11} cm^{-2} while the upper 2DEG density is swept by biasing the central top gate. A constant background has been subtracted from each trace. Calculated critical densities are indicated. Features at the extreme left are associated with the imminent depletion of the upper 2DEG [93]. Copyright (1991) by the American Physical Society. Reprinted with permission of APS and the authors.

diamagnetic shift [108], the above energy can be written as

$$\varepsilon_n(B_x, k_y) = \varepsilon_n + \frac{e^2 B_x^2}{2m}(\langle z \rangle_0 - z_0)^2, \qquad (52)$$

where ε_n is the energy due to the $V(z)$ confining potential in the absence of a magnetic field. We can see, therefore, that equations (50) and (52) yield the approximate result discussed earlier [93] in equations (47) if $\langle z_0 \rangle \to d$, with k_x and k_y appropriately interchanged and the extension is made to the two well system as in that work.

Lyo and Jones [110] showed that further insight into this field configuration can be gained if in equation (48) one assumes a parabolic confining potential, that is, letting $V(z) \to \frac{1}{2} m_z \omega_0^2 z^2$,

in which case equation (48) becomes, including appropriate effective masses,

$$H \to \frac{p_x^2}{2m_x} + \frac{1}{2m_y}(p_y - eB_x z)^2 + \frac{p_z^2}{2m_z} + \frac{1}{2}m_z\omega_0^2 z^2, \tag{53}$$

which can be rewritten as [110]

$$H \to \frac{p_x^2}{2m_x} + \frac{p_y^2}{2m_y^*} + \frac{p_z^2}{2m_z} + \frac{1}{2}m_z\Omega_0^2(z - bp_y)^2, \tag{54}$$

where $m_y^* = m_y\frac{\Omega_z^2}{\omega_0^2}$, $\Omega_z^2 = \frac{m_y\omega^2}{m_z} + \omega_0^2$, $b = \frac{\omega}{m_z\Omega_z^2}$, and $\omega = \frac{eB}{m_y}$. The Schrödinger equation for such a Hamiltonian has an exact solution in the form, $\psi_{n_z,k_x,k_y} = \Phi_{n_z}(z-z_0)\exp[\mathrm{i}(k_y y + k_x x)]$, where the $\Phi_{n_z}(z-z_0)$ are harmonic oscillator solutions in the z direction centred at $z_0 = \frac{\omega\hbar k_y}{m_z\Omega_z^2}$ and eigenvalues $\varepsilon(n_z, k_x, k_y) = \hbar\Omega_z(n_z + \frac{1}{2}) + \frac{(\hbar k_x)^2}{2m_x} + \frac{(\hbar k_y)^2}{2m_y^*}$. This indicates that the effect of the magnetic field in the direction parallel to the TEG layer, under a harmonic confining potential in the z direction, has the effect of producing a field-induced shift in the energy level. The electrons behave like nearly free particles in the x–y plane with a field-dependent enhanced effective mass in the y direction. This model clearly helps to understand how the resonant tunnelling characteristics, such as the NDR regions, shift with an applied magnetic field in the case of a double-barrier system [105]. For the two well system, later work [111] extended their earlier [110] research and used a differential transmission model for the tunnelling conductance with results that compared reasonably well with experiment, under a zero applied bias. In the work of Rainer *et al* [106] the conductance for a double well GaAs/AlGaAs system was investigated under an applied in-plane magnetic field in the presence of a bias voltage. Figure 21 shows a typical result in which the in-plane magnetic field is responsible for a broadening of the resonance structure in the I–V characteristics because tunnelling is allowed for a broad range of energies. All peaks which correspond to transitions into higher unoccupied subbands of their inversion channel shift to higher energies and become asymmetric [106]. The model used to explain their results is similar to that of equations (50) and (52), as discussed before [108] for a two well system and the additional term due to an external bias, in contrast to the Eisenstein *et al* [93] approach, as mentioned in connection to equations (47) for zero bias.

It is important to mention that, in connection to applied magnetic fields in double well systems, the resistance resonance effect mentioned earlier [77] has also been shown to have a magnetic field dependence, referred to as magnetoresistance [80]. For example, in a configuration when the magnetic field is in the direction of the plane of the layers, a longitudinal resistance is observed at a critical field B_c when the current is perpendicular to this field, which is absent when the current is parallel to it. This effect, not surprisingly, is attributed to a difference in the mobilities of the two wells. In that work [80], a Boltzmann equation approach [83], using the symmetric properties of the electron subband dispersion curves, was used to explain the observed phenomena. On the same topic, Berk *et al* [112] studied the behaviour of the resistance resonance [77] as a function of an in-plane magnetic field. The authors found that the in-plane field destroys the coupling between the quantum wells leading to the resistance resonance. Further, the width of the resonance is sensitive to an electron's scattering rate. An in-depth analysis of that work [112] using a Boltzmann kinetic equation approach was later provided [113].

Finally, it is worth noting that, while quantum oscillations in the conductance are due to inter-well tunnelling between Landau levels with the same quantum number [104, 114] in a purely perpendicular magnetic field ($B_\perp$, tunnelling direction), a parallel magnetic field ($B_\parallel$, plane direction) does give rise to conductance oscillations also [115]. This is due to $B_\parallel$ induced oscillations in the overlap integral between harmonic wavefunctions of the quantum wells.

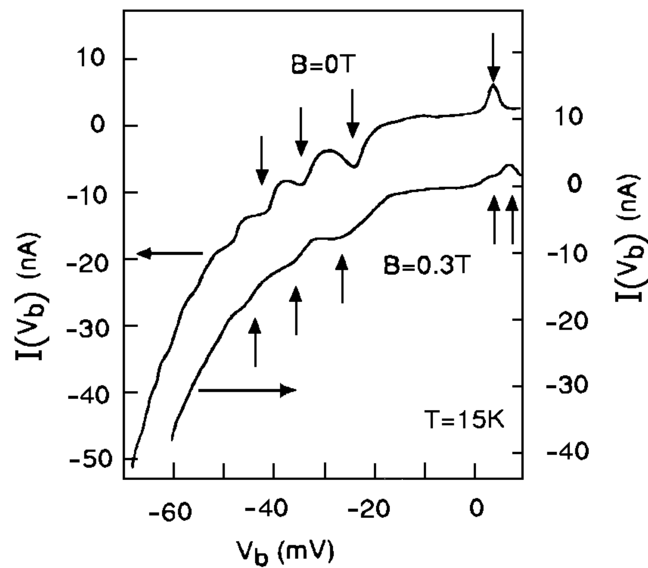

Figure 21. Two typical $I(V_b)$ curves recorded at $T = 15$ K for $B = 0$ T (left scale) and $B = 0.3$ T (right scale). The arrows mark the resonance-peak positions [106]. Copyright (1995) by the American Physical Society. Reprinted with permission of APS and the authors.

5. Conclusion

This review's purpose is to familiarize the reader with the main aspects and interesting points associated with the transport properties of double quantum well systems. The wells consist of two-dimensional (x–y direction) electron gases confined in the z direction. They are separated by a barrier which can be tailored and permits the investigation of quantum phenomena. While the review has mainly been focused on tunnelling conductance aspects between the wells, mention has been made of longitudinal transport properties. In the review, the Wigner function approach, which has been largely applied to double-barrier resonance tunnelling systems, has been compared to the relatively simple approach based on the LF, which in turn was used on an example of a triple-barrier system's conductance. A method to obtain the double well system's wavefunctions was included in which a self-consistent Hartree potential was taken into account in the presence of an electric field. The review includes work in the literature associated with the investigation of the conductance in double well systems in the presence of a magnetic field in the direction of the tunnelling current and perpendicular to it.

This review has not made an attempt to cover topics such as electron correlations in high magnetic fields [116], problems associated with the Coulomb gap [34], the role of electron–electron interactions on electron lifetimes [33, 86, 117, 118], the drag effect [33, 87, 88], the Josephson effect [119] and conductance inhomogeneities related to interface roughness [120] and current distributions [121] in double well systems. Finally, it is important to add that there appears to be a need for more research regarding the fundamental difference in the various transport properties discussed in this review between the double well systems with a single barrier, as in for example [35, 77, 87, 93, 102–104], and those with triple barriers, as for example [32, 38, 69, 122], as originally proposed by Smoliner *et al* [102] and Zohta *et al* [32], respectively.

Acknowledgments

This work was partially supported by an AEG grant no 7826-990228-US from Sun Microsystems Computer Company. The author wishes to thank Dr Peter Price for helpful communications.

References

[1] Cho A Y and Arthur J R 1975 *Prog. Solid. State Chem.* **10** 157
[2] Weimann G and Schlapp W 1985 *Appl. Phys. Lett.* **46** 411
[3] Dingle R, Weigmann W and Henry C H 1975 *Phys. Rev. Lett.* **33** 827
[4] Esaki L 1987 *Physics and Applications of Quantum Wells and Superlattices* ed E E Mendez and K von Klitzing (New York: Plenum) p 1
[5] Tsu R and Esaki L 1973 *Appl. Phys. Lett.* **22** 562
[6] Dingle R 1975 *Festkorperprobleme* vol 15, ed H J Queisser (Oxford: Pergamon) p 21
[7] Sakaki H 1980 *Japan. J. Appl. Phys.* **19** L735
[8] Arakawa Y and Sakaki H 1982 *Appl. Lett.* **40** 939
[9] Hansen W, Kotthaus J P and Merkt U 1992 Nanostructured systems *Semiconduction and Semimetals* vol 35, ed M Reed (New York: Academic) p 279
[10] Dingle R, Stormer H L, Gossard A C and Wiegmann W 1978 *Appl. Phys. Lett.* **33** 665
[11] Hiyamizu S, Saito J, Nambu K and Ishikawa T 1983 *Appl. Phys.* **22** L609
[12] Foxon C T, Harris J J, Hilton D, Hewit J and Roberts C 1989 *Semicond. Sci. Technol.* **4** 582
[13] Reed M (ed) 1992 Nanostructured systems *Semiconduction and Semimetals* vol 35 (New York: Academic)
[14] Powell J L and Crasemann B 1961 *Quantum Mechanics* (New York: Addison-Wesley)
[15] Witkowski L C, Drummond T J, Stanchak C M and Morkoc H 1980 *Appl. Phys. Lett.* **37** 1033
Mimura T, Hiyamuzu S, Fiji T and Kanbu K 1980 *Japan. J. Appl. Phys.* **19** L225
[16] Takikawa M, Komeno J and Ozeki M 1983 *Appl. Phys. Lett.* **43** 280
[17] Guldner Y, Vieren J P, Voisin P, Voos M, Razeghi M and Poisson M A 1982 *Appl. Phys. Lett.* **40** 877
[18] Esaki L and Tsu R 1970 *IBM J. Res. Dev.* **14** 61
[19] Esaki L, Chang L L, Howard W E and Rideout V L 1972 *Proc. 11th Int. Conf. on the Physics of Semiconductors (Warsaw, Poland ed. Polish Academy of Sciences)* (Warsaw: PWN-Polis Sci. Pub.) p 431
[20] Tsu R and Esaki L 1973 *Appl. Phys. Lett.* **22** 562
[21] Chang L L, Esaki L and Tsu R 1974 *Appl. Phys. Lett.* **24** 593
[22] Wolf E L 1985 *Principles of Electron Tunneling Spectroscopy* (New York: Oxford University Press)
[23] Sollner T C L G, Goodhue W D, Tannenwald P E, Parker C D and Peck D D 1983 *Appl. Phys. Lett.* **43** 588
[24] Weisbuch C and Vinter B 1991 *Quantum Semiconductor Structures* (New York: Academic)
[25] Vuong T H H, Tsui D C and Tsang W T 1987 *Appl. Phys. Lett.* **50** 212
[26] Brown R, Goohue W D and Sollner T C l G 1988 *J. Appl. Phys.* **64** 1519
Soderstrom J R, Brown E R, Parker C D, Mahoney L J, Yao J Y, Anderson T G and McGill T C 1991 *Appl. Phys. Lett.* **58** 275
[27] Dalven R 1990 *Introduction to Applied Solid State Physics* (New York: Plenum)
[28] Seeger K 1988 *Semiconductor Physics* (New York: Springer)
[29] Mazumder P, Kulkarni S, Bhattacharya M, Sun J P and Haddad G I 1998 *Proc. IEEE* **86** 664
[30] Datta S 1995 *Electronic Transport in Mesoscopic Systems* (New York: Cambridge University Press)
[31] Kastner M A 1992 *Rev. Mod. Phys.* **64** 849
[32] Zohta Y, Noza T and Obara M 1989 *Phys. Rev.* B **39** 1375
[33] Gusev G M, Gennser U, Maude D K, Portal J C, Rossi J C, Lubyshev D I and Basmaji P 1994 *Solid State Commun.* **91** 105
[34] Turner N, Nicholls J T, Linfield E H, Brown K M, Pepper M, Ritchie D A and Jones G A C 1996 *Solid State Electron.* **40** 413
He S, Platzman P M and Halperin B I 1993 *Phys. Rev. Lett.* **71** 777
[35] Eisenstein J P, Pfeiffer L N and West K W 1991 *Appl. Phys. Lett.* **58** 1497
[36] Wendt J R, Simmons J A, Moon J S, Blount M A, Baca W E and Reno J L 1998 *J. Vac. Sci. Technol.* B **16** 3808
[37] Simmons J A, Blount M A, Moon J S, Lyo S K, Baca W E, Wendt J R, Reno J L and Hafich M J 1998 *J. Appl. Phys.* **84** 5626
Lyo S K 2000 *Phys. Rev.* B **61** 8316
[38] Akyuz C D, Johnson H T, Zaslavsky A, Freund L B and Syphers D A 1999 *Phys. Rev.* B **60** 16597

[39] Howard R E, Hu E L and Jackel L D 1981 *IEEE Electron. Devices* **28** 1378

[40] Ferry D K and Grubin H L 1995 *Solid State Physics–Advances in Applications* vol 49, ed H Erhenreich and F Spaepen (San Diego: Academic) p 283

[41] Barker J R and Ferry D K 1980 *Solid State Electron.* **23** 519
Barker J R and Ferry D K 1980 *Solid State Electron.* **23** 531

[42] Iafrate G J 1992 *Quantum Transport in Semiconductors* ed D K Ferry and C Jacoboni (New York: Plenum) p 53

[43] Ferry D K and Barker J R 1980 *Solid State Electron.* **23** 545

[44] Seiler D G and Stephens A E 1978 *Solid State Electron.* **21** 1

[45] Ferry D K, Barker J R and Jacoboni C (ed) 1980 *Physics of Nonlinear Transport in Semiconductors* (New York: Plenum)

[46] Ferry D K, Barker J R and Grubin H L 1981 *IEEE Electron. Devices* **28** 905
see also,
Hasbun J E 1992 *J. Phys. Chem. Solids* **53** 459
Hasbun J E and Nee T W 1991 *Phys. Rev.* B **44** 3125 and references therein

[47] Hess K 1981 *IEEE Electron. Devices* **28** 937

[48] Teitel S and Wilkins J W 1988 *J. Appl. Phys.* **53** 5006
see also, Hasbun J E 1992 *J. Phys. Chem. Solids* **53** 1305 and references therein

[49] Van Wees B J, Van Houten H, Beenaker C W, Williamson J G, Kowenhoven L P, Van der Marel D and Foxon C T 1988 *Phys. Rev. Lett.* **60** 848

[50] Shah J 1986 *J. Quantum Electron.* **22** 1728

[51] Jacoboni C and Reggiani L 1983 *Rev. Mod. Phys.* **55** 645

[52] Ferry D K 1981 *J. Physique* **42** C7 253

[53] Rammer J 1991 *Rev. Mod. Phys.* **63** 781
Rammer J 1992 *Quantum Transport in Semiconductors* ed D K Ferry and C Jacoboni (New York: Plenum)

[54] Kubo R 1957 *J. Phys. Soc. Japan* **12** 570

[55] Thornber K K and Feynman R P 1970 *Phys. Rev.* B **1** 4099

[56] Kadanoff L and Baym G 1962 *Quantum Statistical Mechanics* (New York: Benjamin)

[57] Wigner E 1932 *Phys. Rev.* **40** 749

[58] Landauer R 1970 *Phil. Mag.* **21** 863

[59] Rossi F, Poli P and Jacoboni C 1992 *Semicond. Sci. Technol.* **7** 1017
see also [51]

[60] Frensley W R 1988 *Superlatt. Microstruct.* **4** 497
Frensley W R 1987 *Phys. Rev.* B **36** 1570

[61] Frensley W R 1990 *Rev. Mod. Phys.* **62** 745

[62] Zhao P, Cui H L, Woolard D, Jensen K L and Buot F A 2000 *J. Appl. Phys.* **87** 1337

[63] Kim K-Y and Lee B 1999 *Solid State Electron.* **43** 81

[64] Kriman A M, Kluksdahl N C, Ferry D K and Ringhofer C 1992 *Quantum Transport in Semiconductors* ed D K Ferry and C Jacoboni (New York: Plenum) p 239

[65] Buttiker M, Pretre A and Thomas H 1993 *Phys. Rev. Lett.* **70** 4114

[66] Sheng L, Xing D Y and Ting C S 1997 *Solid State Commun.* **104** 137

[67] Feng S 1990 *Phys. Lett.* A **143** 400
Meir Y 1999 *Phys. Rev. Lett.* **83** 3506

[68] Landauer R 1987 *Z. Phys.* B **68** 217
Langreth D C and Abrahams E 1981 *Phys. Rev.* B **24** 2978

[69] Zohta Y 1990 *Phys. Rev.* B **41** 7879

[70] Prokofev N, Svistunov B and Tuitsyn I 1999 *Phys. Rev. Lett.* **82** 5092

[71] Lundstrom M 1990 *Fundamentals of Carrier Transport* (New York: Addison-Wesley)

[72] Ando T, Fowler A B and Stern F 1982 *Rev. Mod. Phys.* **54** 437

[73] Landau L D and Lifshitz E M 1977 *Quantum Mechanics* (New York: Pergamon)

[74] Hasbun J E 1995 *Phys. Rev.* B **52** 11989

[75] Hasbun J E and Ban S L 1998 *Phys. Rev.* B **58** 2102

[76] Chevoir F and Vinter B 1993 *Phys. Rev.* B **47** 7261

[77] Palevski A, Beltram F, Capasso F, Pfeiffer L and West K W 1990 *Phys. Rev. Lett.* **65** 1929

[78] Ohno Y, Sakaki H and Tsuchiya M 1994 *Phys. Rev.* B **49** 11492
see also,
Birjulin P I, Grishechkina S P, Ignatiev A S, Kopaev Y V, Shmelev S S, Trofimov V T and Volchkov N A 1997 *Semicond. Sci. Technol.* **12** 427

[79] Vasko F T and Raichev O E 1995 *Phys. Rev.* B **52** 16349
[80] Gompertz M J, Ihn T, Carmona H A, Nogaret A, Main P C, Eaves L, Henini M and Beaumont S P 1996 *12th Int. Conf. on High Magnetic Fields in the Physics of Semiconductors II (Wursburg, Germany)* vol 1 p 445
Ihn T, Carmona H, Main P C, Eaves L and Henini M 1996 *Phys. Rev.* B **54** R2315
[81] Barnes C H W, Davies A G, Zolleis K R, Simmons M Y and Ritchie D A 1999 *Phys. Rev.* B **59** 7669
[82] Vasko F T 1993 *Phys. Rev.* B **47** 2410
[83] Ashcroft N W and Mermin N D 1976 *Solid State Physics* (Philadelphia, PA: Saunders)
[84] Zheng L and MacDonald A H 1993 *Phys. Rev.* B **47** 10619
[85] Lyo S K 2000 *Phys. Rev.* B **61** 8316
[86] Tavares M R S, Hai G-Q and Das Sarma S 2001 *Phys. Rev.* B **64** 045325-1
[87] Gramila T J, Eisenstein J P, Macdonald A H, Pfeiffer L N and West K W 2002 *Phys. Rev. Lett.* **66** 1216
[88] Kellog M, Spielman I B, Eisenstein J P, Pfeiffer L N and West K W 1991 *Phys. Rev. Lett.* **88** 126804-1
[89] Tsuchiya H, Ogawa M and Miyoshi T 1991 *IEEE Trans. Electron. Devices* **38** 1246
[90] Fisher D and Lee P 1981 *Phys. Rev.* B **23** 6851
[91] Callaway J 1991 *Quantum Theory of the Solid State* 2nd edn (San Diego, CA: Academic)
[92] Lyo S K and Simmons J A 1993 *J. Phys.: Condens. Matter* **5** L299
[93] Eisenstein J P, Gramila T J, Pfeiffer L N and West K W 1991 *Phys. Rev.* B **44** 6511
for a detailed theory see [84]
[94] Ban S L, Hasbun J E and Liang X X 2000 *J. Lumin.* **87–89** 369
Ban S L, Hasbun J E and Liang X X 2000 *Acta Sci. Nat. Uni. Nei Mongol* **31** 25
Hasbun J E 2002 *Recent Res. Dev. Phys.* **3** 31
[95] Ando Y and Itoh T 1987 *J. Appl. Phys.* **61** 1497
[96] Burden R L and Faires J D 1989 *Numerical Analysis* 4th edn (Boston, MA: PWS-Kent Pub. Co.)
[97] BenDaniel D J and Duke C B 1966 *Phys. Rev.* **152** 683
[98] Mizuta H and Tanque T 1995 *The Physics and Applications of Resonant Tunneling Diodes* (New York: Cambridge University Press)
[99] Hedin L and Lundquist B I 1971 *J. Phys. C: Solid State Phys.* **4** 2064
[100] Shi J J, Sanders B C and Pan S-H 1999 *Solid State Commun.* **110** 393
Zimmerman B, Marclay E and Llegems M 1988 *J. Appl. Phys.* **64** 3581
[101] Hasbun J E and Roth L M 1988 *Phys. Rev.* B **37** 2829
Nordheim L 1931 *Ann. Phys., Lpz.* **9** 609
[102] Smoliner J, Gornik E and Weimann G 1988 *Appl. Phys. Lett.* **52** 2136
[103] Smoliner J, Gornik E and Weimann G 1989 *Phys. Rev.* B **39** 12937
[104] Smoliner J, Demmerle W, Berthold G, Gornik E and Weimann G 1989 *Phys. Rev. Lett.* **63** 2116
[105] Mendez E E, Esaki L and Wang W I 1986 *Phys. Rev.* B **33** 2893
[106] Rainer G, Smoliner J, Gornik E, Bohm G and Weimann G 1995 *Phys. Rev.* B **51** 17642
[107] Duke C B 1969 *Tunneling in Solids* (New York: Academic)
[108] Demmerle W, Smoliner J, Berthold G, Weiman G and Schlapp 1991 *Phys. Rev.* B **44** 3090
[109] Eisenstein J P, Gramila T J, Pfeiffer L N and West K W 1992 *Surf. Sci.* **267** 377
[110] Lyo S K and Jones E D 1992 *Solid State Commun.* **83** 975
[111] Lyo S K and Simmons J A 1993 *J. Phys.: Condens. Matter* **5** L299
Simmons J A, Lyo S K, Klem J F, Sherwin M E and Wendt J R 1993 *Phys. Rev.* B **47** 15741
[112] Berk Y, Kamenev A, Palevski A, Pfeiffer L N and West K W 1995 *Phys. Rev.* B **51** 2504
[113] Raichev O E and Vasko F T 1996 *Phys. Rev.* B **53** 1522
[114] Gonzalez E M, Lim Y and Mendez E E 2000 *Phys. Rev.* B **63** 033308-1
[115] Lyo S K 1998 *Phys. Rev.* B **57** 9114
[116] Sharpee T, Dykman M I and Platzman P M 2002 *Phys. Rev.* A **65** 032122-1
Dykman M I, Sharpee T and Platzman P M 2001 *Phys. Rev. Lett.* **86** 2408
[117] Murphy S Q, Eisenstein J P, Pfeiffer L N and West K W 1995 *Phys. Rev.* B **52** 14825
[118] Marinescu D C, Quinn J J and Guliani G F 2002 *Phys. Rev.* B **65** 045325-1
[119] Gurvitz S A 1991 *Phys. Rev.* B **44** 11924
Frishman A M and Gurvitz S A 1993 *Phys. Rev.* B **47** 16348
[120] Vasko F T, Balev O G and Studart N 2000 *Phys. Rev.* B **62** 12940
[121] Raichev O E and Vasko F T 1997 *Phys. Rev.* B **55** 2321
[122] Lorke A, Merkt U, Malcher F, Weimann G and Schlapp W 1990 *Phys. Rev.* B **42** 1321
Ferland B, Akyuz C D, Zaslavsky A and Sedgwick T O 1996 *Phys. Rev.* B **53** 994